Geoscience Frontiers 13 (2022) 101090

HOSTED BY

ELSEVIER

Contents lists available at ScienceDirect

Geoscience Frontiers

journal homepage: www.elsevier.com/locate/gsf

Research Paper

Metamorphic gradient modification in the Early Cretaceous Northern Andes subduction zone: A record from thermally overprinted high-pressure rocks

D.S. Avellaneda-Jiménez [a,b,*], A. Cardona [a,c], V. Valencia [d], S. León [a,b,e], I.F. Blanco-Quintero [f]

[a] Grupo de Investigación en Geología y Geofísica (EGEO), Universidad Nacional de Colombia, Medellín, Colombia
[b] Departamento de Materiales y Minerales, Universidad Nacional de Colombia, Medellín, Colombia
[c] Departamento de Procesos y Energía, Universidad Nacional de Colombia, Medellín, Colombia
[d] School of the Environment, Washington State University, Pullman, USA
[e] Smithsonian Tropical Research Institute, Balboa, Ancon, Panama
[f] Departamento de Ciencias de la Tierra y del Medio Ambiente, Universidad de Alicante, Spain

ARTICLE INFO

Article history:
Received 8 November 2019
Received in revised form 11 July 2020
Accepted 25 September 2020
Available online 22 October 2020

Keywords:
Slab roll-back
Mineral chemistry
Phase equilibria
P-T path modeling
Roll-back metamorphism
Thermally overprinted high-pressure rocks

ABSTRACT

New field observations and petrological data from Early Cretaceous metamorphic rocks in the Central Cordillera of the Colombian Andes allowed the recognition of thermally overprinted high-pressure rocks derived from oceanic crust protoliths. The obtained metamorphic path suggests that the rocks evolved from blueschist to eclogite facies towards upper amphibolite to high-pressure granulite facies transitional conditions. Eclogite facies conditions, better recorded in mafic protoliths, are revealed by relic lawsonite and phengite, bleb- to worm-like diopside-albite symplectites, as well as garnet core composition. Upper amphibolite to high pressure granulite facies overprinting is supported by coarse-grained brown-colored Ti-rich amphibole, augite, and oligoclase recrystallization, as well as the record of partial melting leucosomes.

Phase equilibria and pressure-temperature (P-T) path modeling suggest initial high-pressure metamorphic conditions M1 yielding 18.2–24.5 kbar and 465–580 °C, followed by upper amphibolite to high pressure granulite facies overprinting stage M2 yielding 6.5–14.2 kbar and 580–720 °C. Retrograde conditions M3 obtained through chlorite thermometry yield temperatures ranging around 286–400 °C at pressures below 6.5–11 kbar. The obtained clockwise P-T path, the garnet zonation pattern revealing a decrease in X_{grs}/X_{prp} related to Mg# increment from core to rim, the presence of partial melting veins, as well as regional constraints, document the modification of the thermal structure of the active subduction zone in Northern Andes during the Early Cretaceous. Such increment of the metamorphic gradient within the subduction interface is associated with slab roll-back geodynamics where hot mantle inflow was triggered. This scenario is also argued by the reported trench-ward magmatic arc migration and multiple extensional basin formation during this period. The presented example constitutes the first report of Cretaceous roll-back-related metamorphism in the Caribbean and Andean realms, representing an additional piece of evidence for a margin-scale extensional event that modified the northwestern border of South America during the Early Cretaceous.

1. Introduction

The metamorphic record found in subduction-related complexes provides major insights into the long-term tectonic evolution of convergent margins from subduction initiation to the collision of different oceanic and/or continental terranes (Wakabayashi, 2004; García-Casco et al., 2008a, 2008b; Krebs et al., 2008; Escuder-Viruete et al., 2013).

Several petrological studies have been carried out for more than a decade in different Cretaceous metamorphic complexes from the circum-Caribbean region and the Northern Andes (García-Casco et al., 2008a, 2008b; John et al., 2009, among others; Maresch et al., 2009; Blanco-Quintero et al., 2010; Bustamante et al., 2011, 2012; Krebs et al., 2011; Escuder-Viruete et al., 2013; Lázaro et al., 2013, 2016; Escuder-Viruete and Castillo-Carrión, 2016). These studies have been useful for tracking different features along subduction zones, including changes in the thermal regime from hot to cold settings as a consequence of subduction maturity (Krebs et al., 2008, 2011; Blanco-Quintero et al., 2011a), subduction erosion (Escuder-Viruete et al.,

* Corresponding author at: Grupo de Investigación en Geología y Geofísica (EGEO), Universidad Nacional de Colombia, Medellín, Colombia.
E-mail address: dsavellanedaj@unal.edu.co (D.S. Avellaneda-Jiménez).

https://doi.org/10.1016/j.gsf.2020.09.019

2013; Escuder-Viruete and Castillo-Carrión, 2016), and closure of former back-arc basins (Ruíz-Jiménez et al., 2012).

The processes mentioned pre-date the final accretion of oceanic allochthonous terranes and/or continental fragments to the North- and South-American margins during the Late Cretaceous and the Cenozoic (Pindell et al., 2005; García-Casco et al., 2008b; Pindell and Kennan, 2009; Villagómez et al., 2011; Villagómez and Spikings, 2013; Spikings et al., 2015). However, the metamorphic record associated with roll-back or flat-slab geodynamics (e.g. Phillips et al., 2015; Zhang et al., 2017) has not been documented so far in studies conducted along the Caribbean or the Northern Andes, despite its connection with back-arc formation and marginal basin closure, which are common and fundamental elements in the Cretaceous tectonic evolution of these regions (Pindell et al., 2005; Pindell and Kennan, 2009; Escuder-Viruete et al., 2008; Braz et al., 2018; Avellaneda-Jiménez et al., 2019; Zapata et al., 2019).

In the western flank of the Central Cordillera of Colombia, a discontinuous series of Early Cretaceous metamorphic units of medium- (MP) to high-pressure (HP) character crop out (Restrepo and Toussaint, 1976; Orrego et al., 1980; McCourt et al., 1984; González, 1997; Bustamante et al., 2011, 2012; Villagómez and Spikings, 2013; García-Ramírez et al., 2017). These rocks have been associated with either (i) the obduction of oceanic crust (Restrepo and Toussaint, 1976; Toussaint, 1996), (ii) a subduction-accretionary complex system (Villagómez et al., 2011; Bustamante et al., 2012; Spikings et al., 2015; García-Ramírez et al., 2017) or (iii) a continental marginal back-arc basin closure (Ruíz-Jiménez et al., 2012).

The existence of such different tectonic models reflects the limited understanding of the diverse metamorphic record found in these medium- to high-pressure units (McCourt et al., 1984; Bustamante et al., 2012; Ruiz-Jiménez et al., 2012). The lack of precise determination of pressure-temperature-time (P-T-t) paths within these rocks by means of detailed textural-mineralogical and modern thermodynamic methods preclude a proper connection between metamorphism and tectonics, as well as testing the relation between the evolution of the subduction thermal structure and the Early Cretaceous tectonic setting of northwestern South America.

In this contribution, we present field, petrographic and mineral chemistry constraints, together with phase equilibria and P-T path modeling from a HP-MP belt which is part of the Early Cretaceous Arquía Complex (ECAC). This belt crops out in the western flank of the Central Cordillera of Colombia (Fig. 1). The integration of these results with published constraints from other Early Cretaceous metamorphic segments of the ECAC (e.g. Bustamante et al., 2012; Ruiz-Jiménez et al., 2012; García-Ramírez et al., 2017), together with data from the magmatic and sedimentary record of the western Central Cordillera

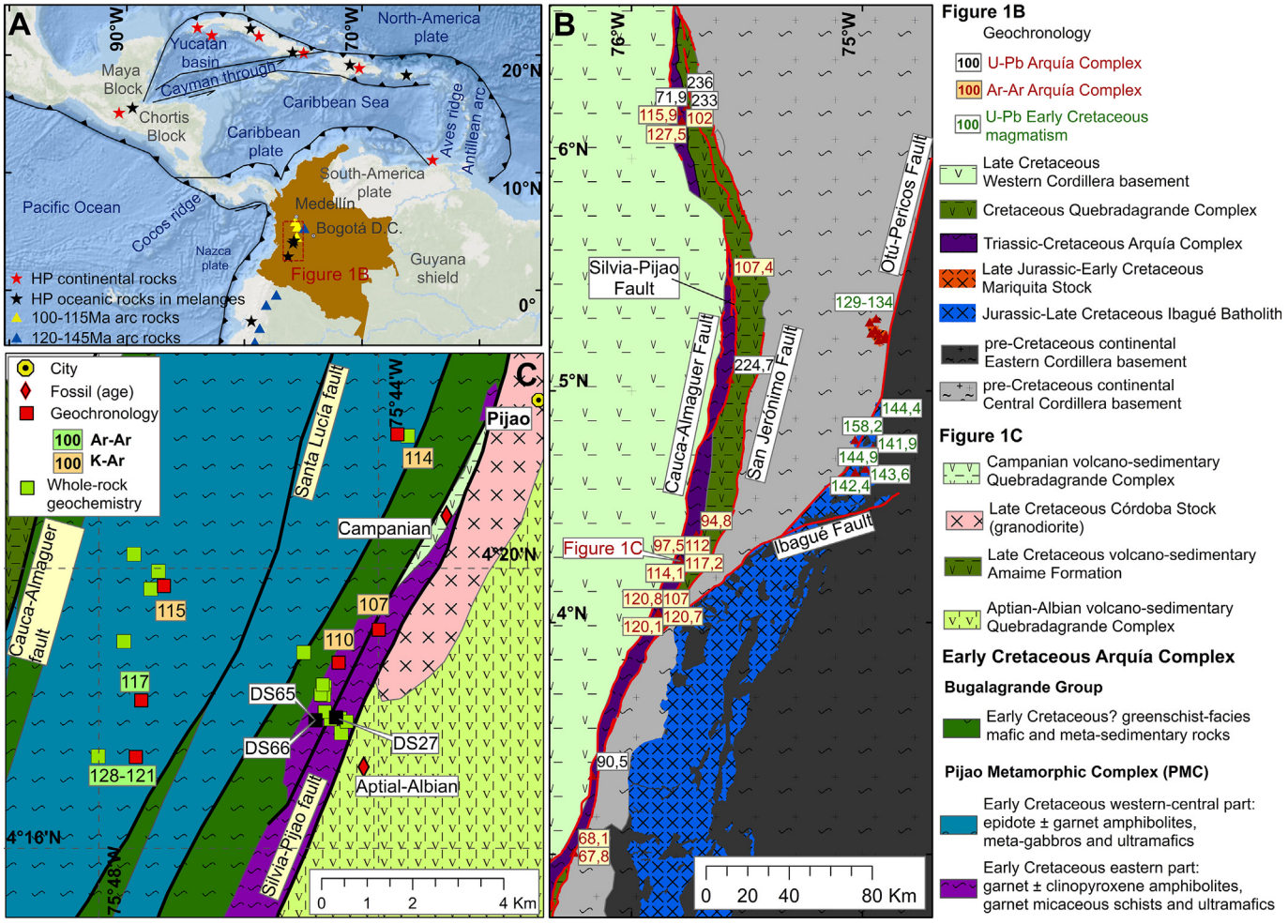

Fig. 1. (A) Northern Andes and Circum-Caribbean region showing Cretaceous high-pressure complexes and Early Cretaceous continental magmatism in the Northern Andes (modified from Avellaneda-Jiménez et al., 2019). (B) Colombian Andes regional map showing the metamorphic Early Cretaceous Arquía Complex cropping out between the Late Cretaceous oceanic Western Cordillera (west) and the back-arc related volcano-sedimentary complex (east). Pre-Cretaceous Central Cordillera continental basement intruded by Jurassic to Early Cretaceous magmatism (modified from Gómez et al., 2014). (C) Geological map from the studied area showing the eastern and western belts in the Pijao Metamorphic Complex discussed in this paper (modified from McCourt et al., 1985). Geochronology and geochemistry after Restrepo and Toussaint (1976), Toussaint and Restrepo (1978), McCourt et al. (1984), Bustamante et al. (2011, 2012), Rodríguez and Arango (2013), Spikings et al. (2015), and Bustamante et al. (2016).

(Villagómez et al., 2011; Rodríguez and Arango, 2013; Villagómez and Spikings, 2013; Avellaneda-Jiménez et al., 2019; Cardona et al., 2019; León et al. 2019; Zapata et al., 2019), allows proposing a better constrained model for the Early Cretaceous tectonic-metamorphic evolution of this unit. Moreover, this can also be used to test regional-scale reconstructions of plate kinematics along the Pacific-South American margin (Spikings et al., 2015; Braz et al., 2018; Zapata et al., 2019).

2. Geological background

The Cretaceous geological record of the Colombian Andes comprises three main tectono-stratigraphic domains with a north to northeast trending. An eastern domain includes the current Eastern Cordillera and the Middle-Upper Magdalena Valley, which are characterized by Berriasian to Aptian clastic and calcareous sediments accumulated in a passive margin suffering extensional episodes (Sarmiento-Rojas et al., 2006).

The western domain, exposed along the current Western Cordillera, includes an oceanic crust basement composed of intercalated oceanic plateau-related basalts with Early- to Middle-Cretaceous marine sediments, which are intruded by ca. 90–80 Ma I-type plutonic rocks with magmatic arc affinity (Kerr et al., 1997; Villagómez et al., 2011; Zapata et al., 2017). This block formed in southern Pacific latitudes as paleomagnetic data suggests (e.g. Hincapié-Gómez et al., 2017) and was accreted to the continental margin between the Late Cretaceous and the Paleocene (Kerr et al., 1997; Villagómez et al., 2011; Villagómez and Spikings, 2013; Spikings et al., 2015; Pardo-Trujillo et al., 2020).

Finally, the central domain represented by the current Central Cordillera and the Cauca Valley, presents a more complex geological record including different metamorphic, volcano-sedimentary and plutonic units. Several Early Cretaceous MP-HP metamorphic rocks, commonly associated with highly serpentinized peridotites, crop out in the westernmost part of this domain and are grouped as part of the ECAC. This belt comprises greenschist- to amphibolite-facies rocks, as well as three major occurrences of high-pressure rocks including blueschists and amphibolized eclogites (González, 1997; Bustamante et al., 2011, 2012; García-Ramírez et al., 2017; Bustamante and Bustamante, 2019; among others).

The volcano-sedimentary units within the central domain include Early Cretaceous siliciclastic sequences accumulated in deltaic to shallow-marine platform environments commonly associated with intermediate to mafic volcanic rocks (Avellaneda-Jiménez et al., 2019; Cardona et al., 2019; León et al., 2019a,b; Zapata et al., 2019). These units are intruded by ca. 98–70 Ma arc-related plutonic rocks and locally covered by Late Cretaceous volcano-sedimentary units, relating their origin to an arc-back-arc setting that was already formed by the Aptian-Albian (Nivia et al., 2006; Villagómez et al., 2011; Cochrane et al., 2014; Spikings et al., 2015; Jaramillo et al., 2017; Avellaneda-Jiménez et al., 2019; León et al. 2019; Zapata et al., 2019; among others).

2.1. Early Cretaceous Arquía Complex (ECAC)

The MP-HP metamorphic rocks associated with ultramafic units exposed in the western flank of the Central Cordillera and the Cauca Valley were originally grouped under the name of Arquía Complex (AC; Maya and González, 1995).

Geochronological data, including amphibole K—Ar, amphibole and white mica Ar—Ar, and garnet-whole-rock Lu—Hf ages, together with whole-rock geochemistry and petrological constraints from some units within this complex (Restrepo and Toussaint, 1976; Toussaint and Restrepo, 1978; McCourt et al., 1984; Bustamante et al., 2011, 2012; Villagómez and Spikings, 2013; García-Ramírez et al., 2017), allows discrimination of at least two different Cretaceous metamorphic events (Bustamante and Bustamante, 2019).

The first event is Early Cretaceous in age and is recorded by blueschists, amphibolized eclogites, and MP amphibolite-facies rocks that have been related to different tectonic settings as mentioned above. A younger Late Cretaceous event has been recognized by widespread greenschist facies meta-volcanic and meta-gabbroic rocks, with 63–71 Ma white mica Ar—Ar cooling ages obtained from retrograded blueschist-facies rocks (Bustamante et al., 2011; Bustamante and Bustamante, 2019 and reference therein). The Late Cretaceous event has been related to the subduction and subsequent collision between Cretaceous intra-oceanic units currently forming part of the Western Cordillera, and the South America continental margin (Bustamante et al., 2011; Bustamante and Bustamante, 2019).

These rocks are bounded to the east by the dextral Silvia-Pijao regional fault (Fig. 1; Maya and González, 1995), which defines the tectonic limit with respect Early Cretaceous volcano-sedimentary rocks formed within a back-arc setting (Zapata et al., 2019; Avellaneda-Jiménez et al., 2019 and reference therein). This and other strike-slip faults associated with the Romeral fault system seems to have displaced the blocks tens to hundreds of kilometers northward (e.g., Pindell and Kennan, 2009; Bayona et al., 2010; Montes et al., 2019).

2.2. Pijao metamorphic complex (PMC)

A metamorphic complex included within the ECAC crops out in the western flank of the Central Cordillera between 4°N and 4.5°N latitude near Pijao town (Fig. 1C). In this area, the available map of this complex includes the Rosario Amphibolites and the Bugalagrande Group (McCourt et al., 1984). The Rosario Amphibolites was mapped and described as a prominent mafic amphibolite- to eclogite-facies metamorphic unit composed of ± garnet amphibolites, meta-gabbros, and serpentinized peridotites enclosing amphibolized eclogite fragments (McCourt et al., 1984, 1985).

The Bugalagrande Group represents a greenschist to epidote-amphibolite facies intercalation of meta-sedimentary and meta-volcanic rocks (Fig. 1C; McCourt et al., 1984). Fieldwork and petrography of the latter suggest a not genetically related metamorphic history with respect the Rosario Amphibolites, supported by different composition, especially in sedimentary protoliths showing high quartz content, lower metamorphic grade with no progressive transition towards the Rosario unit, and a prominent mylonitic texture which could be the result of regional shearing during younger events.

In this contribution, we focus in rocks formerly associated with the Rosario Amphibolites. However, we informally refer to this unit as the Pijao Metamorphic Complex (PMC) considering the lithologically heterogeneous nature of the unit, including HP metapelites, thermally overprinted eclogites, and associated leucosomes suggesting partial melting of some rocks which were not described before.

To avoid misinterpretation and generalization of the metamorphic history presented in this paper to the entire AC, we divided the PMC into two belts. A western belt includes garnet amphibolites, meta-gabbros, and amphibolitic schists from which the main feature is showing prograde MP metamorphism with no evidence of an earlier HP stage. On the other hand, the eastern belt, aim of this work, is composed of thermally overprinted HP rocks (interlayered meta-sedimentary and meta-mafic rocks) as will be presented below (Figs. 1C and 2).

Retrograde eclogites within the eastern belt have been previously reported as centimeter- to meter-size bodies with lenticular geometries enclosed within garnet-amphibolites (García-Ramírez et al., 2017). In this work, we show not only the existence of retrograde eclogites, but also upper amphibolite to high pressure granulite transitional facies overprinted eclogites.

Several highly serpentinized and fault-bounded peridotites crop out in the eastern part of both belts. These ultramafic rocks are usually tens to hundreds of meters in size and do not form regional and continuous belts. They are always observed as westward thrusted lenticular bodies over the metamorphic rocks, commonly cropping out at the tectonic boundaries between the PMC and the Bugalagrande Group. The ultramafic rocks may be interpreted as

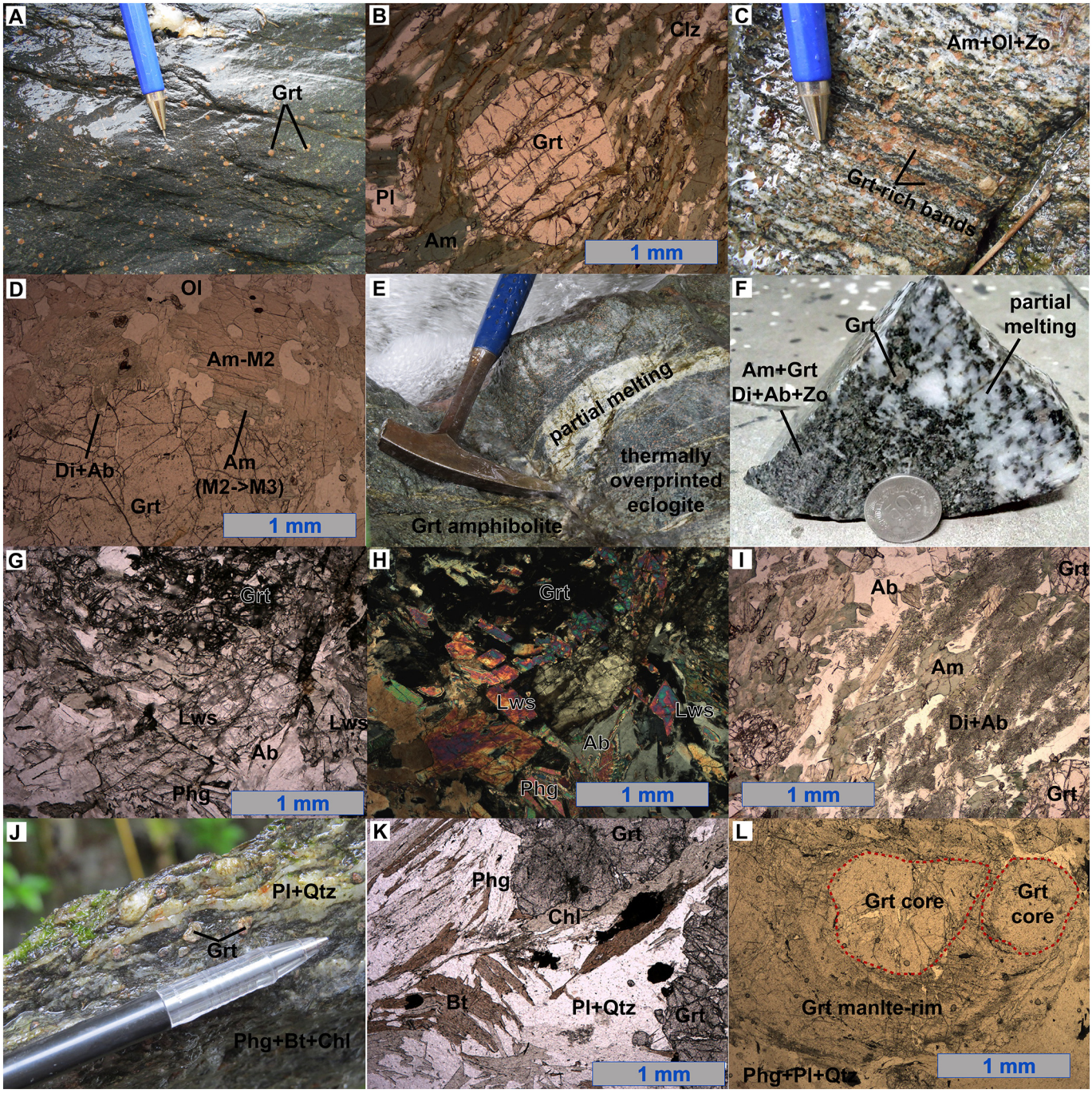

Fig. 2. Field view and photomicrographs of different samples associated with the western (A, B) and eastern (C–L) belts of the PMC. (A, B) Field view of fresh garnet amphibolite and photomicrograph of garnet amphibolite showing well-defined foliation and prograde amphibolite-facies metamorphism. (C, D) Field view and photomicrographs of sample DS27 (thermally overprinted eclogite) showing typical coarse-grained texture, garnet-rich bands, diopside + albite symplectites (M1- > M2) and green-colored amphibole rimming brown-colored amphibole cores (M2- > M3). (E–I) Field view and photomicrographs of sample DS65, thermally overprinted eclogites pods enclosed within garnet amphibolite showing leucocratic veins/pods associated with partial melting (E and F). Lawsonite and phengite relics of M1, and diopside + albite symplectites of M1- > M2 transition is also shown (H and I). (J–L) Field view and photomicrographs of sample DS66 (metapelite) showing well-defined schistose texture, decussate texture in biotites and some white micas, and garnet rim enclosing two different garnet cores.

fragments of the mantle wedge which was incorporated within the subduction channel during the exhumation event. Hence, they did not experience HP and MT metamorphism.

Available whole-rock geochemical data from the PMC suggest an oceanic-crust protolith so far, which include N-MORB and *E*-MORB affinity (Villagómez et al., 2011; Rodríguez and Arango, 2013; García-Ramírez et al., 2017). Geochronological data includes for the eastern belt, an eclogite-facies metamorphic peak age of ca. 129 Ma through Lu—Hf garnet-whole-rock isochron (García-Ramírez et al., 2017) and 115–110 Ma cooling K—Ar ages obtained from amphiboles (Toussaint and Restrepo, 1978; McCourt et al., 1985). The western belt comprises 107–117 Ma K-Ar and Ar—Ar cooling ages from amphiboles in prograde MP rocks (McCourt et al., 1985; Villagómez and Spikings, 2013).

Pre-Albian protolith formation of PMC is primarily constrained by eclogites-facies peak and cooling ages, whereas Aptian metamorphism and at least partial exhumation of the unit is constrained by its erosion detected in the adjacent Aptian-Albian sedimentary rocks of the westernmost Central Cordillera (Avellaneda-Jiménez et al., 2019).

3. Material and methods

3.1. Fieldwork and petrography

Fieldwork was conducted across the western flank of the Central Cordillera near the locality of Pijao (Fig. 1C). Despite the dense vegetation and intense weathering, relatively fresh samples were collected for petrographic, geochemical and mineral chemistry analyses.

A total of 40 thin sections from the PMC were characterized under the polarized light petrographic microscope. Three representative samples from the eastern belt of the PMC, including two upper amphibolite to high pressure granulite transitional facies overprinted eclogites (samples DS27 and DS65) and a thermally overprinted HP metapelite (sample DS66) were chosen for mineral chemistry, elemental X-ray maps, phase equilibria, and P-T path modeling. Mineral assemblages and textures of these samples preserve HP mineral relics and document the subsequent thermal overprint, as well as greenschist to epidote-amphibolite facies retrograde stage. These three metamorphic assemblages (facies) are referred as M1, M2, and M3, respectively.

3.2. Mineral chemistry and elemental X-ray maps

Mineral chemistry and elemental X-ray maps were acquired using a CAMECA SX-50 electron microprobe at the Department of Lunar and Planetary Sciences at the University of Arizona, USA. Mineral chemical analyses were performed with a beam current of 20.0 nA and an accelerating voltage of 15 kV. Counting peak time was 20 s for all elements. Elemental X-ray maps were done at 15 kV, 40 nA, 10 ms dwell time, and 3 μm step size, with a resolution of 1024 pixels per line. The standards used for element calibrations were “albite-Cr” for Na, “ol-fo92” for Mg and Si, “anor-hk” for Al and Ca, “kspar-OR1” for K, “rutile1” for Ti, “fayalite” for Fe, “rhod-791” for Mn and “chrom-s” for Cr (see http://rruff.info/about/downloads/Normal_UofA_Standards.pdf for standard abbreviation).

Garnet and clinopyroxene compositions were normalized to 8 cations/12 oxygens and 4 cations/6 oxygens respectively; Fe^{3+} was estimated by stoichiometry. Feldspar was normalized to 8 oxygens and assuming Fe^{total} as Fe^{3+}. White mica and chlorite were normalized to 11 and 28 oxygens respectively and assuming Fe^{total} as Fe^{2+}. Amphibole was normalized to 24 oxygens, and its classification and Fe^{3+} calculation was following Hawthorne et al. (2012) and Locock (2014). Mg# is $Mg/(Mg + Fe^{2+})$, Fe# is $Fe^{2+}/(Mg + Fe^{2+})$, and An is $Ca/(Ca + Na)$. Analytical results are presented in Appendix A.

Garnet chemistry discussed in this manuscript was initially used by Avellaneda-Jiménez et al. (2019) for provenance analysis, but it is presented in Appendix A to include the distance information (mm) of chemical profiles.

3.3. Whole-rock geochemistry

For phase equilibria modeling, major oxides of the selected samples were obtained by Inductively Coupled Plasma Atomic Emission Spectroscopy (ICP-AES) at the ALS Mineral laboratories in Vancouver Canada. For each sample, 0.1 g were well-mixed and fused within a lithium metaborate/lithium tetraborate flux (1.8 g) in a furnace at 1000 °C. The resulting melt was then cooled and dissolved in 100 mL of an acid mixture containing 4% nitric and 2% hydrochloric acids. The derived solution was then analyzed by ICP-AES. Sample locations and analytical results are presented in Appendix B.

3.4. Phase equilibria and P-T path modeling

For phase equilibria analysis, we used the software Perple_X version 6.8.8 (Connolly, 2005), considering the more recent internally consistent thermodynamic datasets from Holland and Powell (1998, 2003, and subsequent updates). A MnNCKFMASH-O system was established for all samples, assuming a fluid phase in excess being pure H_2O only at high pressure conditions (M1 stage). O_2 content was established through mineral proportion and composition within specific stability fields using T-O_2 diagrams at constant pressure, whereas H_2O content for M2 was calculated using the pseudosection at peak M1 conditions. The conditions are presented in Appendix B.

For all samples, the used solution models for garnet, chlorite, and white mica are based on White et al. (2014), whereas for feldspar and epidote the models are after Holland and Powell (2003) and Holland and Powell (1998) respectively. For mafic rocks, solution model for amphibole is after Dale et al. (2005), clinopyroxene after Green et al. (2007), and melt solution after Green et al. (2016). For the metapelite (DS66) the biotite solution model is after White et al. (2014) whereas the melt solution is after White et al. (2001).

These solution models were chosen considering applied examples from rocks with similar metamorphic histories as the one discussed by this work (e.g. Faryad et al., 2019). Although all samples were taken from regions of the outcrops with no adjacent leucosomes (in order to study not fractionated materials), considering the possibility of melt migrations two scenarios were modeled, not considering a melt solution and involving the latter.

Isochemical P–T projections (pseudosections) were constructed for each sample using whole-rock geochemistry presented in Appendix B. The method presented by Evans (2004) and Gaidies et al. (2006) was used for calculating the percentage of garnet core fractionation for each sample, in order to account for the implications that fractionation and effective bulk composition may have on phase equilibria modeling. Garnet core fractionation was applied for calculating M2 conditions.

Samples DS27 and DS65 (mafic rocks) gave values of 4.5 wt% and 1.1 wt% garnet core fractionation respectively, whereas sample DS66 (metapelite) yielded 0.6 wt% garnet fractionation. High pressure conditions M1 were calculated using unfractionated phase equilibria modeling for all samples, whereas M2 stage was obtained using a second pseudosection modeling based on effective bulk composition after garnet core fractionation. Garnet core and effective bulk compositions for phase equilibria modeling are presented in Appendix B. Mineral abbreviations are after Siivola and Schmid (2007).

4. Results

The eastern belt is composed of interlayered biotite + garnet + white mica schists (metapelites), coarse-grained ± augite + diopside + garnet amphibolites, and amphibolized lawsonite bearing eclogites (Fig. 2). Plagioclase-rich leucosomes with igneous textures occur as centimeter-size veins and/or pods within several meta-mafic rocks suggesting partial melting (Fig. 2E and F). Leucocratic segregates are interpreted as *syn*-metamorphic due to the absence of crenulation, cuspate textures around garnet and some amphiboles, and intergranular trapped melt textures (Appendix D). These segregates show concordant to cross-cutting relationships with the main foliation of the host rocks (Fig. 2F).

The belt shows a main foliation striking N25°–65°E and dipping 35°-85°SE. A crenulation axial plane with strike varying between N20°W to N15°E and dipping 50°–78° to the east is locally observed usually near local inverse faults.

4.1. Textural and mineral assemblage evolution

Samples DS27 and DS65 are mafic in composition, although sample DS65 is a 1-m lenticular body enclosed within a garnet amphibolite with

partial melting leucosomes (Fig. 2E). These rocks are mainly composed of amphibole (42–45 vol%), garnet (20–24 vol%), diopside/augite (4–8 vol%), oligoclase/albite (8–15 vol%), quartz (4–7 vol%), clinozoisite/zoisite (6–8 vol%), phengite (1–4 vol%), chlorite (1–4 vol%), lawsonite (< 1 vol%), and accessory minerals are rutile, titanite and ilmenite/magnetite (Fig. 2).

Sample DS27 is a coarse-grained rock showing a well-defined gneissic texture with garnet-rich bands intercalated with amphibole + oligoclase + clinozoisite/zoisite + minor garnet domains (Fig. 2C). Sample DS65 is a medium-grained rock showing an anastomosed schistose texture defined by amphibole, but locally, some amphibole and phengite grains present decussate textures (Fig. 2G–I).

Sample DS66 is a metapelitic rock with well-defined schistosity (Fig. 2J) interlayered with overprinted eclogites (sample DS65). The metapelite is composed of phengite (40 vol%), garnet (20 vol%), quartz (15 vol%), chlorite (10 vol%), biotite (8 vol%) and plagioclase (7 vol%). Rutile is the most common Ti-phase showing always ilmenite/magnetite rims. Phengite and biotite locally show a decussate texture near the garnet porphyroblasts (Fig. 2K). Chlorite is always rimming biotite.

4.1.1. Early HP stage (M1)

This stage is recorded in the mafic rocks (samples DS27 and DS65) by relic lawsonite and diopside + albite symplectites. Lawsonite is rare but it is preserved as small crystals (<0.5 mm) within garnet porphyroblasts pressure-shadows and as inclusions in core and few rims from the latter (Fig. 2G and H). Former lawsonite is also interpreted from tabular/rhombic clinozoisite showing textural equilibrium with phengite aggregates resembling lawsonite pseudomorphs (c.f., Tsujimori and Ernst, 2014).

Fine-grained diopside + albite symplectites showing bleb- to worm-like textures are interpreted as breakdown products of former omphacite (Figs. 2I and 3; Zhao et al., 2001; Song et al., 2003; Zhang et al., 2017). Coarse-grained omphacites rimmed by these types of symplectites have been described in eclogites within the study area by García-Ramírez et al. (2017).

HP mineral relics have not been recognized within the metapelitic sample (DS66) but considering that it was collected from the same outcrop (interlayered) than sample DS65, we consider that the subsequent overprinting stages erased in high amount the earlier HP mineral assemblage.

Garnet core growth within mafic rocks is associated with this stage since it contains lawsonite and phengite inclusions, whereas garnet core of the metapelitic rock could be associated to this stage mostly based on its chemical composition and elements ratios, but also by considering phengite and rutile inclusions within the core while chlorite and biotite inclusions only at the mantle-rim.

In mafic rocks the garnet grains are up to 3 mm in size and are highly fractured presenting zoisite, amphibole, albite, and rutile inclusions as well (Figs. 2 and 3). Zoisite and amphibole inclusions are presented in the mantle-rim together with rutile showing titanite rims, providing a non-clear connection with the M1 stage. Diopside + albite symplectites are also observed as inclusions within the garnet rim, but always are associated with irregular garnet fractures connecting the symplectites with the matrix (Figs. 2 and 3). This feature suggests post-trapping reactions associated with fluid entering along fractures given the pervasive symplectite development in the matrix. This symplectites are then associated with M1 to M2 transition as discussed below.

Garnets are almandine- ($0.45 < X_{alm} < 0.59$) and grossular-rich ($0.26 < X_{grs} < 0.38$) in composition, showing differences in pyrope

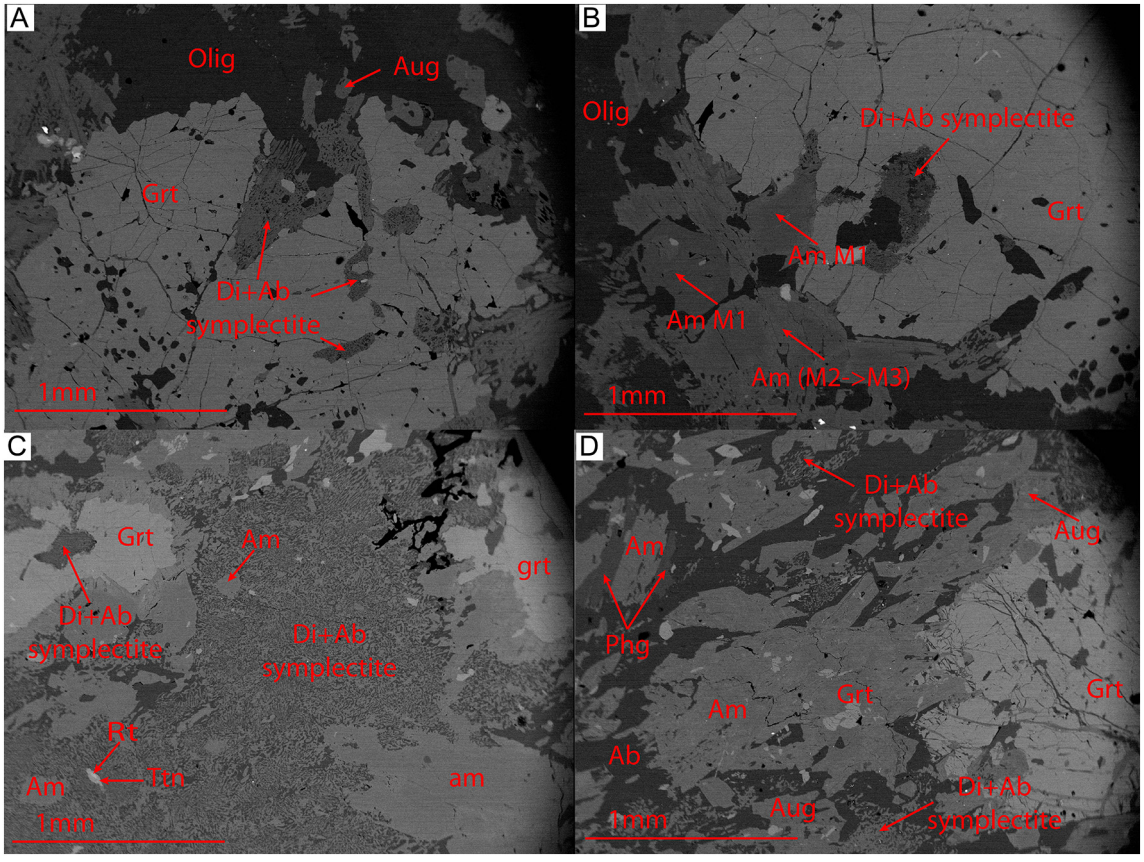

Fig. 3. Backscattered electron images of samples DS27 (A, B) and DS65 (C, D) showing bleb- and worm-like symplectites of diopside + albite. Note that symplectites included in garnet are always associated with fractures connecting garnet mantle-rim with the matrix.

and spessartine content (Appendix A). Sample DS27 shows garnet with higher pyrope ($0.19 < X_{prp} < 0.23$) and lower spessartine content ($0.01 < X_{sps} < 0.03$) than sample DS65 ($0.07 < X_{prp} < 0.17$; $0.01 < X_{sps} < 0.11$). Mg# ranges between 0.28 and 0.32 and 0.12–0.25 in samples DS27 and DS65 respectively (Appendix A). Elemental X-ray maps (Fig. 4A and B) and compositional profiles (Fig. 5) reveal that garnets from mafic rocks are characterized by a slight decrease in X_{sps}, constant X_{grs} and X_{alm}, and slight increase in X_{prp} (Fig. 5A and B). These features suggest diffusion modification of garnet during M2. Estimated conditions attained during M1 based on garnet core composition are hence, to some extent, uncertain.

In the metapelite (sample DS66) garnet shows sizes up to 4 mm and commonly are characterized by clean cores and opaque-inclusion poikiloblastic rims (Fig. 2L). Some garnet porphyroblasts show poikiloblastic overgrowth enclosing two different garnet cores (Fig. 2L). Garnet shows high almandine ($0.59 < X_{alm} < 0.83$), with

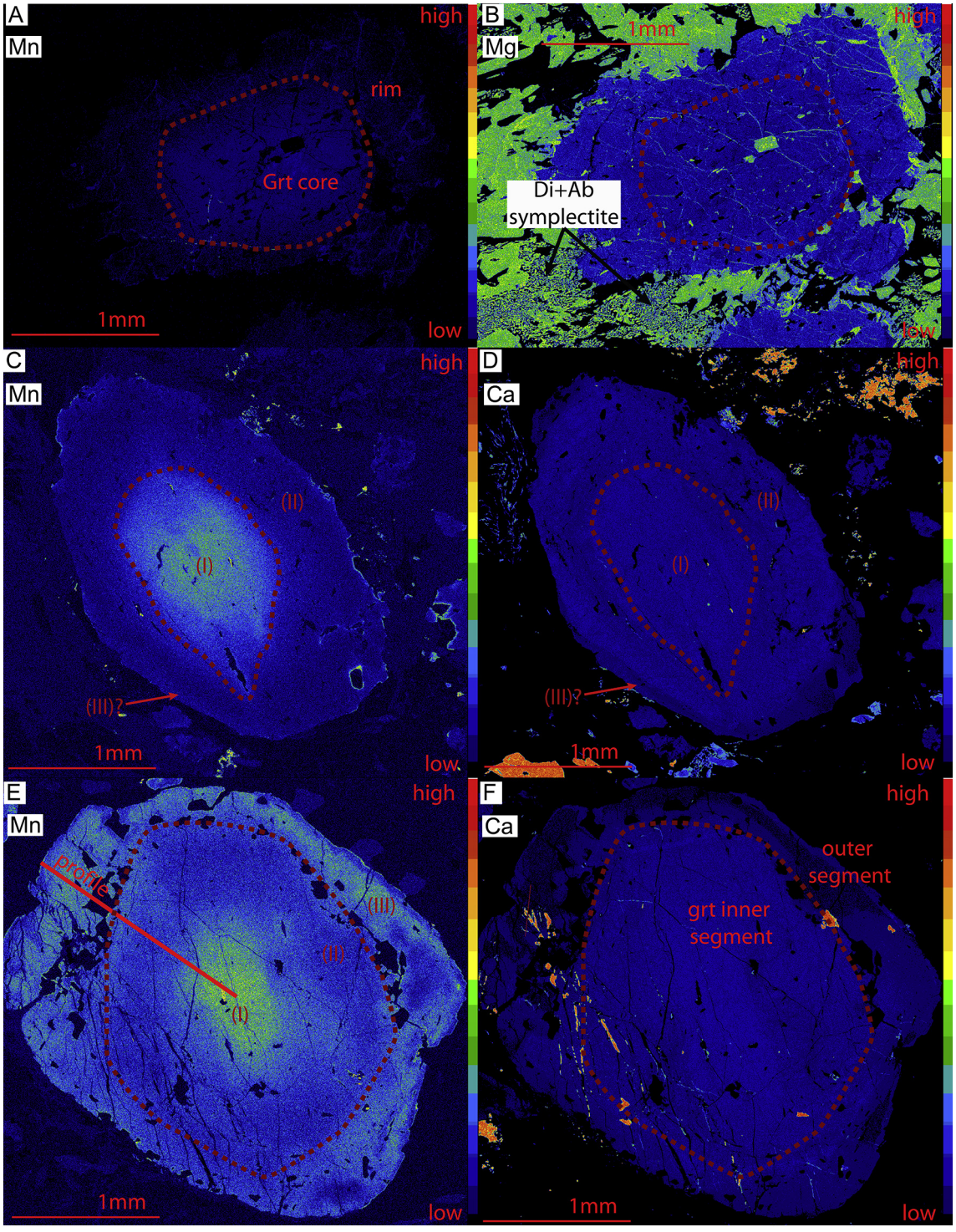

Fig. 4. Elemental X-Ray garnet maps. (A, B) Sample DS65 (eclogite). (C, D) Type-1 garnet in sample DS66 (metapelite). (E, F) Complex zoning pattern associated with type-2 garnet from sample DS66. See text for details and Appendix D for extra maps.

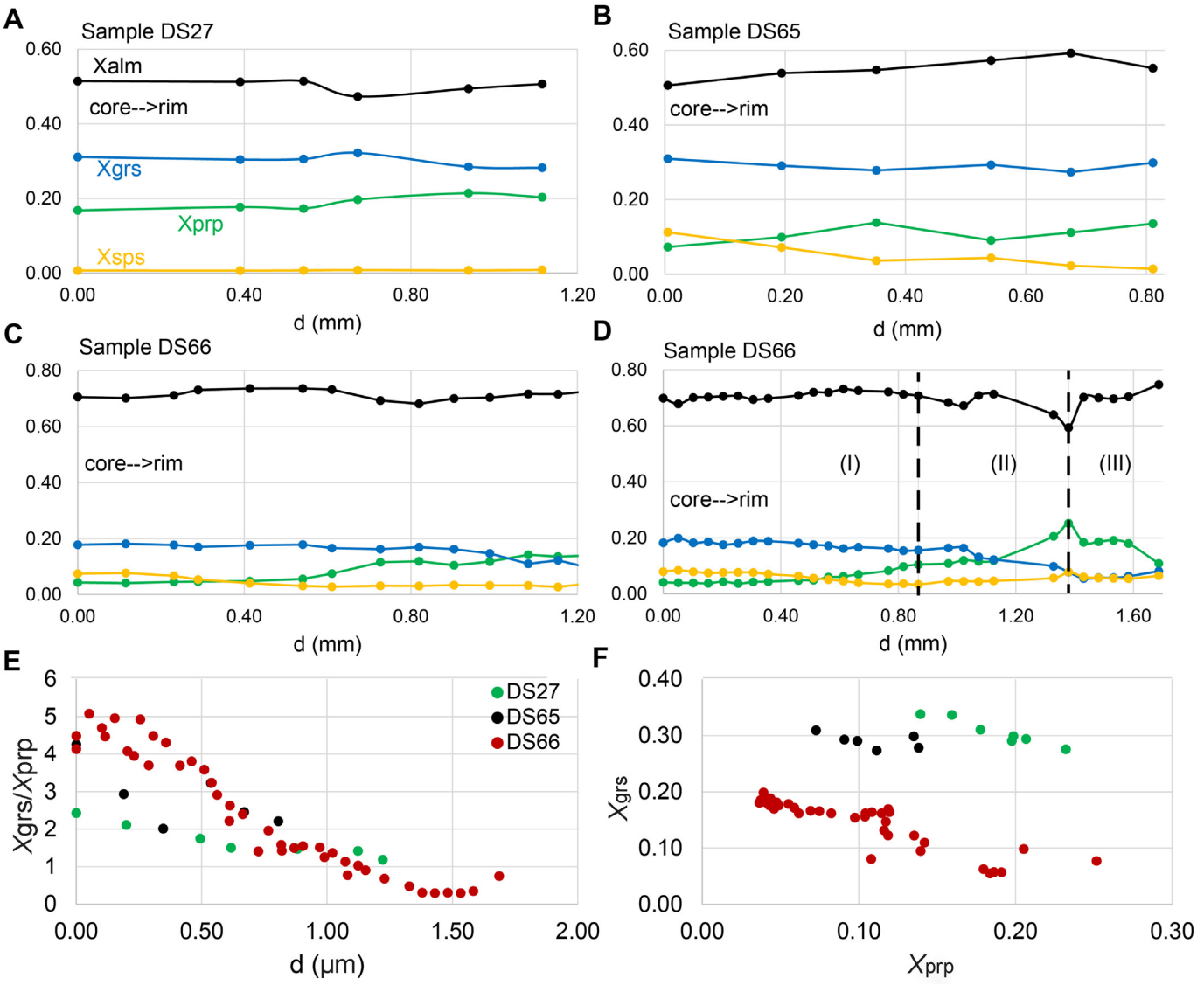

Fig. 5. Garnet composition and chemical variation. (A, B) Samples DS27 and DS65 respectively (thermally overprinted eclogites). (C, D) Sample DS66 (metapelite). (E) X_{grs}/X_{prp} decrement from core to rim. (F) X_{grs} decrement and X_{prp} increment associated with X_{grs}/X_{prp} decrement from core to rim.

$0.04 < X_{prp} < 0.25$ and $0.05 < X_{grs} < 0.20$ content; spessartine (X_{sps}) and Mg# range 0.01 to 0.08 and 0.05 to 0.30 respectively (Appendix A).

Two types of garnets are discriminated from the metapelitic rock (Figs. 4C–F and 5; Appendix D). Type-1 garnet shows a compositional pattern similar to the described for mafic rocks, but with a more pronounced X_{sps} decrease and X_{prp} increment from core to rim (Figs. 4C, D and 5C). Type-2 garnet, with a diameter over 2.4 mm, shows complex zoning patterns allowing subdivision into two segments (inner and outer) and three growing stages (I-III). Stage I is associated with M1 whereas stage III with M2. Stage II is link to the transition between M1 and M2 as discussed below.

Elemental X-ray maps (Fig. 4C–F) and compositional profile (Fig. 5C and D) shows an inner segment with X_{sps}, X_{grs}, and X_{alm} decrease, together with increment in X_{prp} from core (stage I) to rim (stage II). The outer segment also shows increment in the amount and size of quartz inclusions (Fig. 4E and F); composition of the latter is presented in the M2 description.

4.1.2. Thermally overprinted stage (M2)

This stage is recorded by the appearance of augite, Ti-rich amphibole, and oligoclase in mafic rocks, whereas in the metapelite by garnet rim composition with biotite inclusions and biotite stability with phengite in the matrix (Figs. 2 and 3). Associated to this stage is also the breakdown of rutile into titanite and ilmenite for mafic rocks and metapelite respectively, and although not addressed in detail in this work, partial melting also argues for thermal overprinting as well (Fig. 2E and F).

Augite (Fig. 6) occurs in sample DS65 as grains within the matrix in contact with albite, and as small grains within Di + Ab symplectites (Fig. 3). Augite shows low Na (0.05–0.10 apfu) and Jd (0.13–0.19) content, with Wo ranging 0.27–0.29, En 0.43–0.46, and Fs 0.25–0.30 (Appendix A). Mg# ranges 0.59–0.65.

Amphibole has variable chemical composition. Sample DS27 shows pargasite-tschermakite composition for matrix grains whereas inclusions within garnet are magnesio-hornblende and ferri-tschemakite in composition (Fig. 7B). Amphibole inclusions occur within the mantle-rim of garnet, but due to fractures connecting these inclusions with the matrix as well as their similar composition to matrix amphibole, they are related to M2 stage rather than M1. Post-trapping reactions associated with fluid entering along those fractures is also suggested by inclusions of Di + Ab symplectites in garnet as mentioned before.

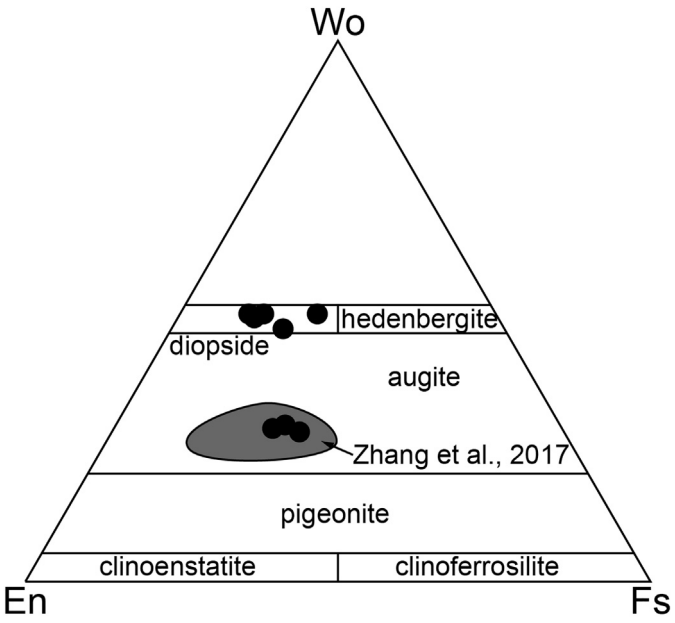

Fig. 6. Pyroxene classification of thermally overprinted eclogite DS65 (diagram after Morimoto, 1988).

Sample DS65 shows pargasitic matrix amphibole (Fig. 7A and B; Hawthorne et al., 2012), which is always green-colored and occurs as well-developed individual grains associated with diopside + albite symplectites (Figs. 2I and 3). Si ranges from 6.05 to 6.76 and 6.43 to 6.91 apfu in samples DS27 and DS65 respectively, with Ti between 0.02 and 0.06 apfu (Fig. 7C, Appendix A). Ti-rich amphibole is brown in color and only found in sample DS27 (Fig. 2D), they show Ti content between 0.10 and 0.11 apfu (Fig. 7C).

Plagioclases are sodic-rich, showing oligoclase composition ($0.77 < X_{ab} < 0.87$) for sample DS27 and albite composition ($0.92 < X_{ab} < 1.00$) for both samples (Fig. 7D). Oligoclase is associated with Ti-rich amphibole whereas albite is found within diopside bearing symplectites.

Within sample DS27, the An content in plagioclase increases from core to rim. Ca—Na relation shows a negative slope pattern, with Ca and Na varying between 0.07 and 0.23 and 0.79–0.93 for sample DS27 while 0.01–0.08 and 0.94–1.02 for sample DS65 (Fig. 7D; Appendix A).

Garnet rim within the metapelitic rock (outer segment in Fig. 4E and F) is associated with this stage. This segment related with the third growth-stage (Fig. 5D) is characterized by X_{sps}, X_{grs} and X_{alm} increase, and constant X_{prp} and Mg# content. A thin outermost rim shows X_{prp} and Mg# depletion as well (Fig. 5D).

4.1.3. HP to thermally overprinted stage transition (M1- > M2)

The transition between M1 and M2 (M1- > M2) is recorded in mafic rocks by former omphacite breakdown into diopside + albite in stability with phengite (Figs. 2 and 3), whereas in the metapelite by biotite inclusions within the garnet mantle-rim and the association biotite + phengite + ilmenite in the matrix.

Diopside associated with symplectites within mafic rocks is only recorded in sample DS65 (Figs. 2 and 3), showing low Na content (0.08–0.14 apfu) with Al between 0.06 and 0.16 apfu, and Jd between 0.15 and 0.27 (Appendix A). Wo is 0.49 while En and Fs range 0.37–0.40 and 0.11–0.13 respectively; Mg# ranges 0.83–0.84 (Appendix A).

Phengite from mafic sample DS65 associated with this stage is rich in Si (3.24–3.32 apfu), Mg (0.24–0.28 apfu), and Fe (0.09–0.11 apfu) (Fig. 8A; Rieder et al., 1998), with K between 0.73 and 0.85 apfu and low Na content ranging from 0.06 to 0.12 apfu (Appendix A). Phengites from metapelitic rock show Si, Mg, and Fe values varying from 3.15 to 3.35 apfu, 0.12 to 0.28 apfu, and 0.09 to 0.14 apfu, respectively, with K between 0.76 and 0.88 apfu and Na content between 0.07 and 0.10 apfu (Appendix A). No Pg composition was obtained from the acquired data, but we do not discharge its presence as discussed below.

A negative-sloped of X_{grs}/X_{prp} ratio from core to rim is observed from garnets in all samples (Fig. 5E); this decrement is associated with X_{grs} decrement and X_{prp} increment (Fig. 5F). Considering that X_{grs}/X_{prp} ratio can be used as a qualitative proxy for dP/dT modification, we associate this compositional trend to the M1- > M2 transitional stage, accompanying diopside + albite symplectite development (decompression) and augite, Ti-rich amphibole, and biotite crystallization (prograde conditions).

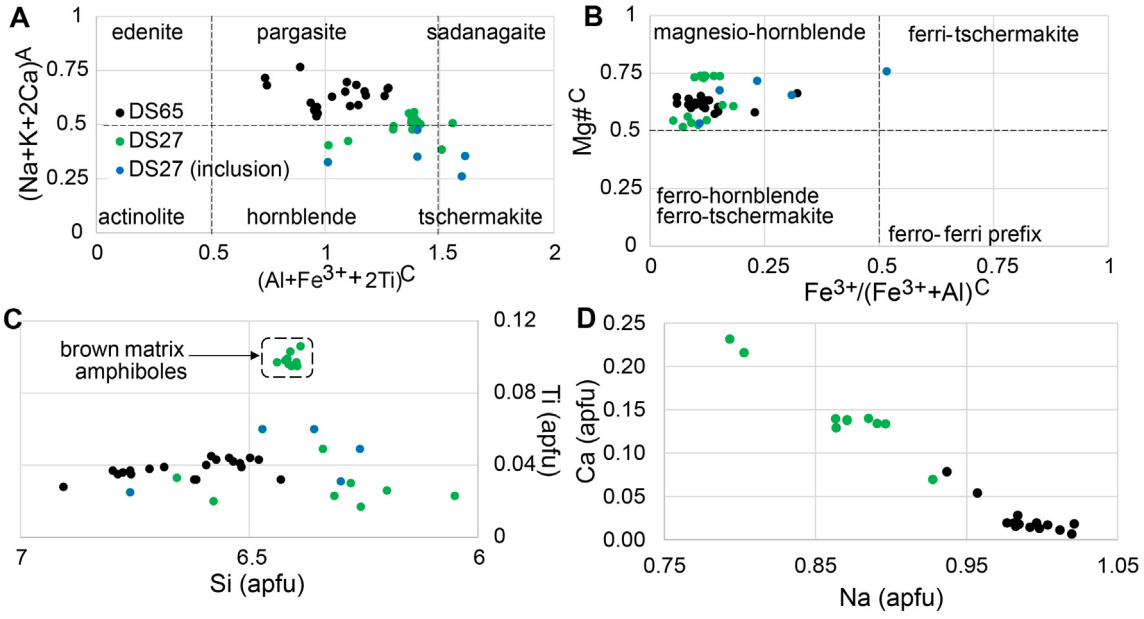

Fig. 7. (A, B) Amphibole classification and composition from overprinted and retrograde mafic eclogites. (C) Ti content in amphiboles from samples DS27 and DS65. Brown-colored and Ti-rich amphiboles are from sample DS27. (D) Plagioclase composition in samples DS27 and DS65.

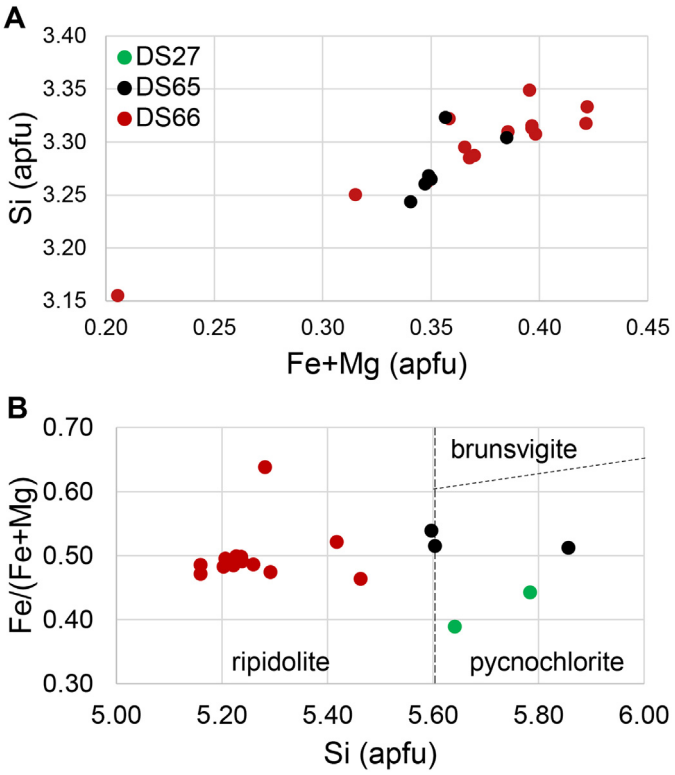

Fig. 8. (A). Phengite composition showing high Si and Fe + Mg content in samples DS65 (thermally overprinted eclogite) and DS66 (metapelite) (Rieder et al., 1998). (B) Chlorite classification after Hey (1954) showing ripidolite to pycnochlorite composition.

4.1.4. Retrogression (M3)

Amphibolite facies associated with slight temperature decrease is recorded in mafic rocks by green-colored magnesio-hornblende rimming brown-colored Ti-rich amphiboles (Fig. 2D). Strong retrograde stage M3 is defined by chlorite replacing calcium-rich amphibole and garnet in mafic rocks whereas biotite in the metapelite (Figs. 2 and 3).

Chlorite shows ripidolite and pycnochlorite compositions in the mafic samples and ripidolite composition in the metapelite (Fig. 8B; Hey, 1954). In mafic rocks, the Si and Fe# vary from 5.64 to 5.78 apfu and 0.39 to 0.44 for sample DS27, whereas 5.60 to 5.86 apfu and 0.51 to 0.54 for sample DS65 respectively (Appendix A). Chlorite grains from sample DS66 (metapelite) show Si and Fe# ranging from 5.16 to 5.46 apfu and 0.46 to 0.64 respectively (Appendix A).

4.2. Phase equilibria and P-T path modeling

4.2.1. Sample DS27

The M1 stage was calculated using unfractionated phase equilibria through X_{grs} (0.30–0.34), Mg# (0.21–0.29) and X_{sps} (0.01–0.02) garnet isopleths within the Grt + Wmca + Cpx + Am + Lws + Qtz stability field of the pseudosection presented in Fig. 9A. The field assemblage is consistent with the preserved inclusions in garnets (Fig. 3). Isopleths intersection yielded 19.5–21.8 kbar and 525–580 °C.

Using fractionated phase equilibria based on 4.5 wt% garnet core fractionation and recalculated water content (1.7 wt%), M2 stage was constrained by intersection of Mg# in amphibole (0.68–0.74) and X_{An} (0.13–0.23) in oligoclase isopleths. Conditions without involving a melt model yielded 10.8–13 kbar and 670–720 °C within the Grt + Wmca + Pl + Cpx + Am + Zo + Qtz stability field of the pseudosection presented in Fig. 9B, whereas similar 10.5–12.5 kbar and 590–640 °C within the Grt + Wmca + Cpx + Am + Pl + Zo + Qtz + melt were calculated when a melt solution was involved (Fig. 9C). However, at these conditions a low melt proportion (6–12 vol%) are formed as is expected (Figs. 9C and 2E, F). P-T conditions are similar for both scenarios, considering that no partial melting leucosomes were observed near the sample, it suggests migration of the liquid if melting was achieved.

The above conditions define a clockwise P-T path from eclogite facies towards the upper amphibolite to high pressure granulite facies transitional field, also supported by the increment of Mg# in garnet rim (III in Fig. 4) and the brown amphibole showing cores with low Ti (0.02–0.06 apfu) and higher Ti content of 0.10–0.11 apfu at rims (Raase, 1974).

Amphibole thermometry based on Ti content shows temperatures ranging 565–618 °C for low Ti whereas 659–673 °C for higher Ti content (Appendix C; Otten, 1984). These calculations could represent minimum temperatures due to Ti-availability, which in this case is controlled by Rt stability, allowing amphibole with a not maximum amount of titanium (Otten, 1984). The latter is in accordance with empirical TiO_2 in amphibole thermometry showing temperatures between 500 and 600 °C for the low Ti amphibole and 650–730 °C for higher Ti content (Ernst and Liu, 1998).

Retrograde conditions M3 below 10.5 kbar and 298–322 °C is suggested by the lower pressure estimates for M2 and chlorite thermometry (Appendix C; Cathelineau, 1988; Jowett, 1991).

4.2.2. Sample DS65

The M1 stage was calculated using unfractionated phase equilibria through X_{grs} (0.29–0.32), Mg# (0.12–0.20) and X_{sps} (0.02–0.04) garnet isopleths within the Grt + Wmca + Cpx + Am + Lws + Chl stability field of the pseudosection presented in Fig. 10A. Isopleths intersection yielded 22–24.5 kbar and 500–540 °C.

Using fractionated phase equilibria considering a 1.1 wt% of garnet core fractionation and water recalculation (2.4 wt%), M2 stage was calculated by Mg# in augite (0.59–0.65) and amphibole (0.57–0.65), and X_{An} (0.02–0.08) in albite. Conditions without involving a melt model yielded 11–14.3 kbar and 580–640 °C within the Grt + Wmca + Pl + Cpx + Am + Zo + Qtz stability field of the pseudosection presented in Fig. 10B, whereas similar 11–14.2 kbar and 600–660 °C within the Grt + Wmca + Pl + Cpx + Am + Zo + melt were obtained when a melt solution was involved (Fig. 10C). Less than 12 vol% of melts was calculated at M2 conditions within the latter setup (Fig. 10C). P-T conditions are similar for both scenarios, partial melting leucosomes were observed near the obtained sample (Fig. 2E), so probably the melting model is more accurate.

The above conditions define a clockwise P-T path from eclogites facies towards the upper amphibolite to high-pressure granulite facies transitional field in accordance with sample DS27. Amphibole thermometry based on Ti content shows temperatures ranging 578–600 °C in accordance with empirical TiO_2 in amphibole thermometry showing temperatures between 500 and 600 °C (Appendix C; Otten, 1984; Ernst and Liu, 1998). As mentioned before, these temperatures represent minimum temperatures due to Ti-availability (Otten, 1984).

Retrograde conditions M3 below 11 kbar and 286–333 °C is suggested by the lower pressure estimates for M2 and chlorite thermometry (Appendix B; Cathelineau, 1988; Jowett, 1991).

4.2.3. Sample DS66

The M1 stage was calculated using unfractionated phase equilibria through X_{grs} (0.16–0.22), Mg# (0.04–0.06) and X_{sps} (0.02–0.08) garnet core (stage I) isopleths within the Grt + Wmca + Pg + Chl + Lws + Jd + Gln + Rbk + Qtz stability field of the pseudosection presented in Fig. 11A. The isopleths intersection yielded stability conditions of 18.2–19.8 kbar and 465–485 °C.

The stability field suggests lawsonite together with sodic clinopyroxene and amphiboles (Gln and Rbk) for the M1 assemblage, considering that those phases were not observed within the petrography we interpret that they must be in low proportion within the outcrop or entirely erased as a consequence of M2 and M3 overprinting and retrograde stages respectively.

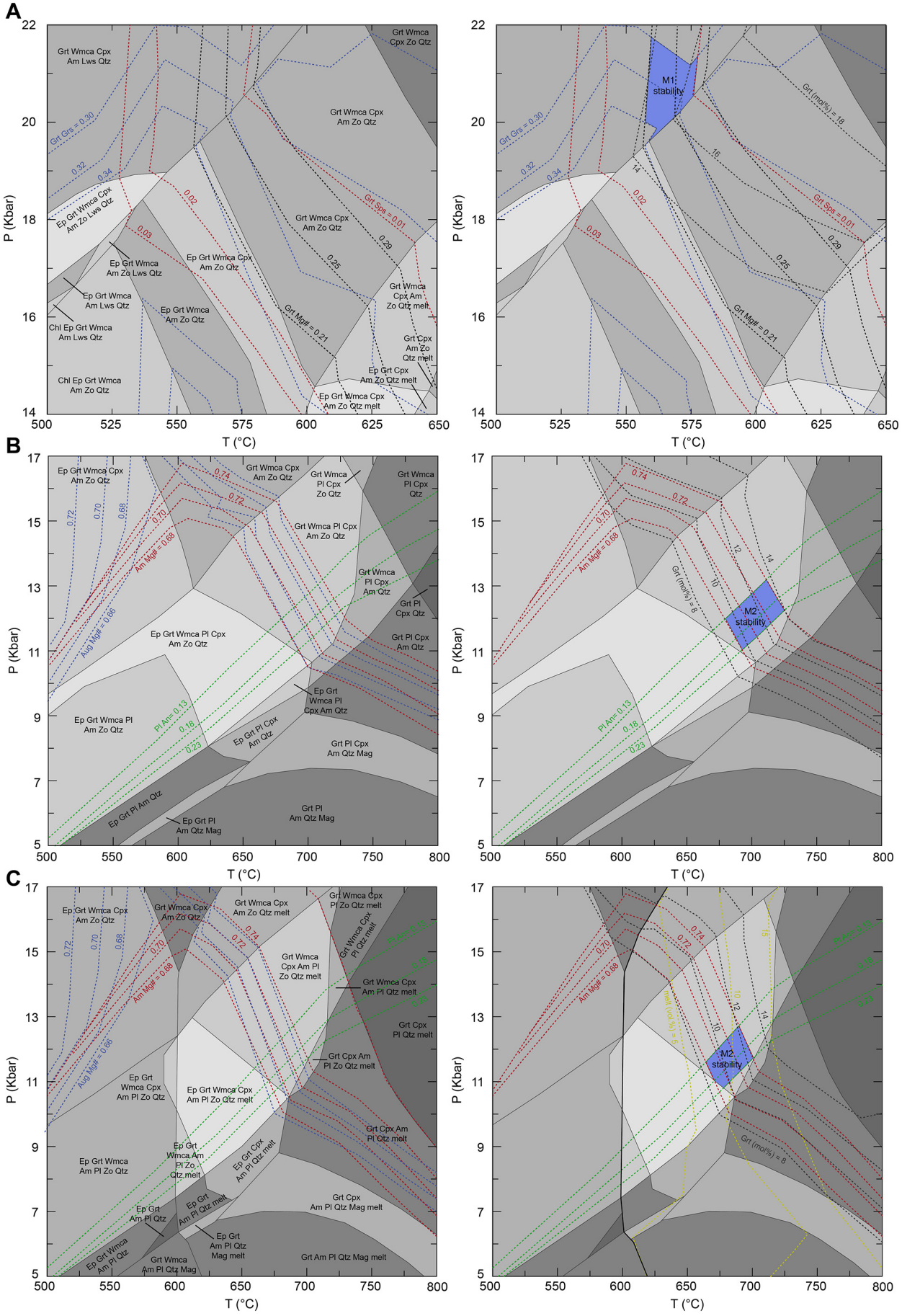

Fig. 9. Pseudosection modeling of sample DS27 (thermally overprinted eclogite). (A) HP M1 stage; (B) M2 stage considering 4.5 wt% of garnet core fractionation without using a melt model; (C) Same as (B) involving a melt solution model. See text for details.

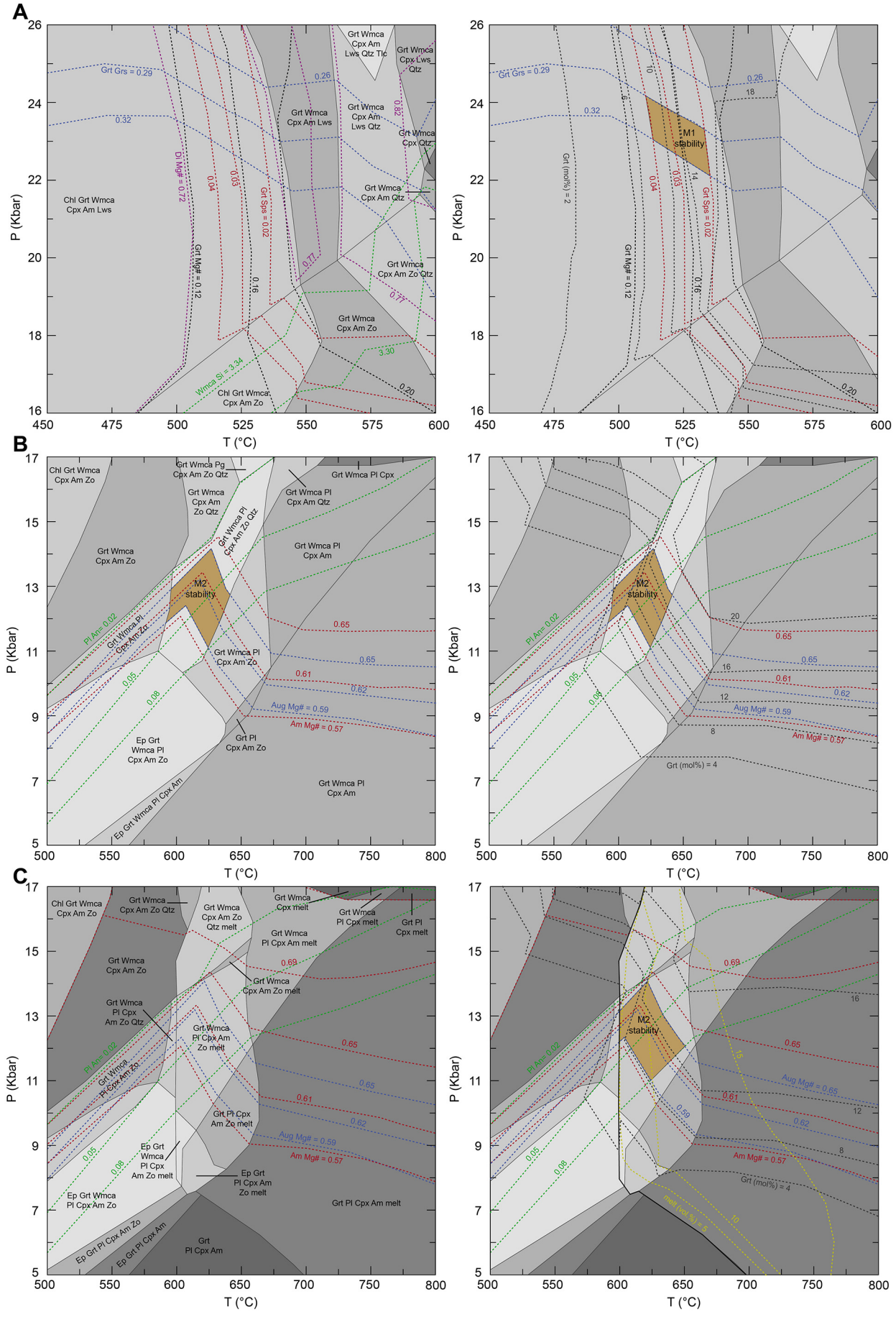
A
B
C
P (Kbar)
T (°C)
Chl Grt Wmca Cpx Am Lws
Grt Wmca Cpx Am Lws
Grt Wmca Cpx Am Lws Qtz Tlc
Grt Wmca Cpx Lws Qtz
Grt Wmca Cpx Am Lws Qtz
Grt Wmca Cpx Qtz
Grt Wmca Cpx Am Qtz
Grt Wmca Cpx Am Zo Qtz
Grt Wmca Cpx Am Zo
Chl Grt Wmca Cpx Am Zo
Grt Grs = 0.29
0.32
0.26
0.82
0.77
0.16
0.20
3.30
Wmca Si = 3.34
Grt Sps = 0.02
Grt Mg# = 0.12
Di Mg# = 0.72
0.04
0.03
M1 stability
Grt (mol%) = 2
10
6
14
18
Chl Grt Wmca Cpx Am Zo
Grt Wmca Pg Cpx Am Zo Qtz
Grt Wmca Cpx Am Zo Qtz
Grt Wmca Pl Cpx Am Qtz
Grt Wmca Pl Cpx
Grt Wmca Pl Cpx Am Zo Qtz
Grt Wmca Pl Cpx Am
Grt Wmca Pl Cpx Am Zo
M2 stability
Pl Am= 0.02
0.65
0.61
0.62
0.09
0.08
Aug Mg# = 0.59
Am Mg# = 0.57
Grt Pl Cpx Am Zo
Ep Grt Wmca Pl Cpx Am Zo
Ep Grt Wmca Pl Cpx Am
Grt Wmca Pl Cpx Am
Grt (mol%) = 4
20
16
12
8
Grt Pl Cpx melt
Grt Wmca Cpx melt
Grt Wmca Pl Cpx melt
Grt Wmca Cpx Am Zo melt
Grt Wmca Pl Cpx Am melt
Grt Wmca Pl Cpx Am Zo melt
Grt Pl Cpx Am Zo melt
Ep Grt Wmca Pl Cpx Am Zo melt
Ep Grt Pl Cpx Am Zo melt
Grt Pl Cpx Am melt
Ep Grt Pl Cpx Am Zo
Ep Grt Pl Cpx Am
Grt Pl Cpx Am
0.69
0.59
0.15
melt (wt %) = 5
10

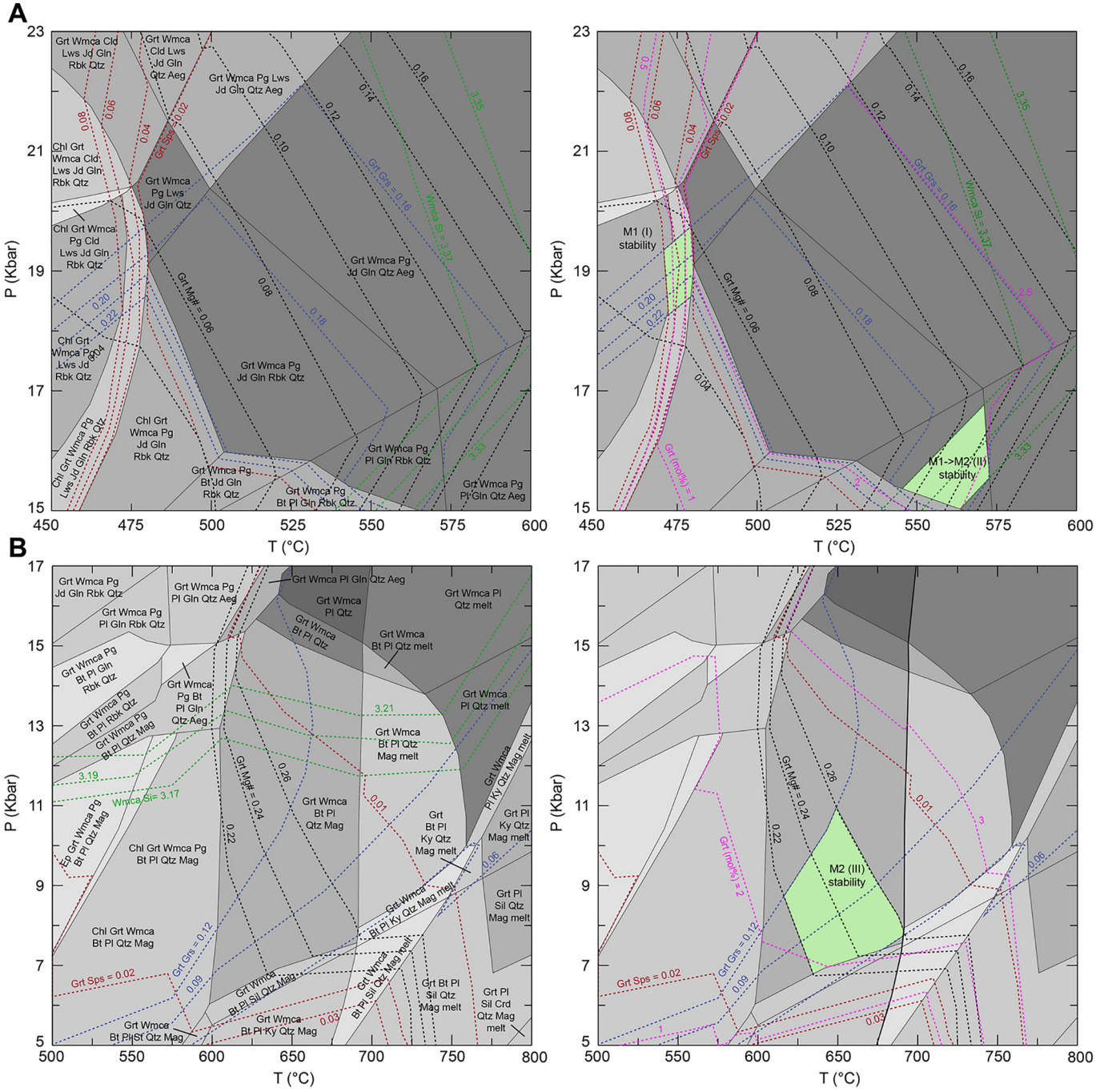

Fig. 11. Pseudosection modeling of sample DS66 (thermally overprinted metapelite). (A) HP M1 stage; (B) M2 stage considering 0.6 wt% of garnet core fractionation involving a melt solution model. See text for details.

On the other hand, M1- > M2 transition was constrained through X_{grs} (0.16–0.18) and Mg# (0.12–0.14) in garnet mantle (stage II) and Si content (3.30–3.34 apfu) in phengite isopleths, yielding 15–16.8 kbar and 540–570 °C within the Grt + Wmca + Bt + Pl + Qtz + Mag stability field of the pseudosection presented in Fig. 11A. This is in accordance with the entrance of biotite in equilibrium with phengite observed as inclusions within garnet mantle and rim.

Using fractionated phase equilibria considering a 0.6 wt% of garnet core fractionation and recalculated water content (1.5 wt%), M2 stage was calculated by X_{grs} (0.06–0.12), Mg# (0.22–0.26), and X_{sps} (0.01–0.02) garnet rim isopleths within the Grt + Wmca + Bt + Pl + Qtz + Mag stability field of the pseudosection presented in Fig. 11B. Isopleths intersection yielded 6.5–11 kbar and 620–690 °C. The model involving a melt solution for M2 suggest no melting conditions for this sample.

Fig. 10. Pseudosection modeling of sample DS65 (thermally overprinted eclogite). (A) HP M1 stage; (B) M2 stage considering 1.1 wt% of garnet core fractionation without using melt model. (C) Same as (B) involving a melt solution model. See text for details.

The above results define a clockwise P-T path from blueschist to eclogite facies towards the upper amphibolite to high pressure granulite facies transitional field. Retrograde conditions M3 below 6.5 kbar and 348–400 °C is suggested by the lower pressure estimates for M2 and chlorite thermometry (Appendix B; Cathelineau, 1988; Jowett, 1991).

5. Discussion

5.1. Metamorphic evolution

Phase equilibria and P-T path modeling supported by petrographic textures and mineral chemistry, show that samples from the eastern belt of the PMC record a major HP event (M1) overprinted by upper amphibolite to HP granulite transitional facies conditions (M2) (Fig. 12). This overprinted stage was followed by greenschist to epidote-amphibolite facies retrograde stage M3, defined by chlorite recrystallization replacing in different degrees amphibole, garnet, and biotite.

The M1 stage yielding 18.2–24.5 kbar and 465–580 °C together with lawsonite and high-Si phengite relics, support blueschist to eclogite facies metamorphism associated with a metamorphic gradient below 10 °C/km (Appendix C). These results can be associated with metamorphism within cold and mature subduction-related tectonic settings (Ernst, 1988; Spear, 1993; Wakabayashi, 2004).

As discussed above, all samples show a clockwise P-T path describing a thermally overprinting stage M2 (Fig. 12). This M2 stage yielding 6.5–14.3 kbar and 580–720 °C, suggests a temperature increment during initial pressure drop. These conditions argue for rocks evolving from high-pressure conditions in a cold metamorphic gradient (<10 °C/km) to hotter conditions within the upper amphibolite to HP granulite facies transition within a metamorphic gradient between 10 and 30 °C/km (Fig. 13; Appendix C).

The latter is in accordance with higher temperatures shown by brown amphiboles with higher Ti content towards the rim (Otten, 1984; Ernst and Liu, 1998) and garnets showing a well-developed negative sloped X_{grs}/X_{prp} pattern and Mg# enrichment from core to rim, were the latter argues for a progressive lowering of the metamorphic gradient (dT/dP) during prograde garnet growth. The increment in temperature during initial decompression, constrained by X_{grs} variation and diopside + albite symplectites development, is also suggested by partial melting of augite bearing mafic rocks (Fig. 2E and F).

The retrograde stage M3 is characterized by pressures below 6.5–11 kbar and temperatures between 286 and 400 °C (Appendix C). The latter is interpreted as strong and final greenschist to epidote-amphibolite facies retrograde stage associated with the final exhumation event of the subduction-related complex.

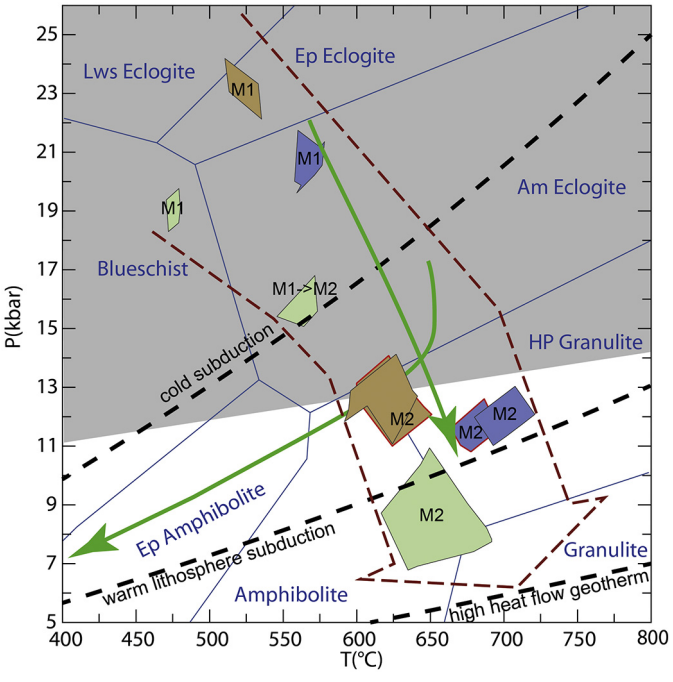

Fig. 12. P-T paths from the eastern belt in PMC compared to subduction-related metamorphism during roll-back geodynamics (green path; Phillips et al., 2015). High-pressure event M1 took place in a cold (<10 °C/km) metamorphic gradient, while upper amphibolite to HP granulite facies overprinting stage is associated with hotter gradients (10–30 °C/km). Metamorphic facies and HP field (grey) after Liou et al. (2004). Cold and warm subduction, as well as high heat flow geotherms after Ernst (2010). See text for discussion.

5.2. Tectonic implications

Mafic protoliths from the PMC have been interpreted as oceanic crustal derived rocks with MORB-like geochemical signatures including data from the eastern belt (Villagómez et al., 2011; Rodríguez and Arango, 2013; García-Ramírez et al., 2017). This oceanic crust was subducted during the late Jurassic to early Cretaceous (Bustamante and Bustamante, 2019 and reference therein), allowing HP metamorphism (M1) under a cold-metamorphic gradient (< 10 °C/km).

The M1 stage took place nat around 129 Ma as supported by Lu—Hf garnet geochronology in eclogites cropping out within the studied area (García-Ramírez et al., 2017). This age is linked to the cold conditions as suggested by the provided petrographic description showing high proportion of garnet (40 vol%) and omphacite (25 vol%), together with poor symplectite development around the latter (García-Ramírez et al., 2017). Associated with this subduction complex an active continental margin was contemporaneously producing arc-related magmatism between 145 and 129 Ma (Spikings et al., 2015; Bustamante et al., 2016; Rueda-Gutiérrez, 2019), supporting an Early Cretaceous east-dipping subduction system.

Upper amphibolite to HP granulite facies overprinting of former eclogites implies a relative increase of temperature during initial exhumation. This path could be associated with (i) slow rates of exhumation (O'Brien and Rötzler, 2003), (ii) flat-slab tectonics (Zhang et al., 2017), (iii) oceanic ridge subduction (Blanco-Quintero et al., 2010), or (IV) the modification of the thermal structure during ongoing subduction due to asthenospheric inflow (Phillips et al., 2015; Laurent et al., 2018; Faryad et al., 2019; Sizova et al., 2019).

As mentioned before, provenance constraints from the Albian-Aptian sandstones of the adjacent volcano-sedimentary rocks reveals erosion and sediment supply from the eastern belt of the PMC, suggesting that this unit was at least partially exposed on surface by ca. 118 Ma (Avellaneda-Jiménez et al., 2019). This feature (erosion of the ECAC) has been also observed in provenance analyses conducted on coeval sedimentary rocks exposed farther to the north in the western flank of the Central Cordillera (León et al., 2019a).

Considering the ca. 129 Ma Lu—Hf peak metamorphic age in eclogite (García-Ramírez et al., 2017), the calculated 18.2–24.5 kbar HP conditions, and the near 118 Ma exhumation-erosion of the metamorphic belt, it is possible to estimate a range in exhumation rates. The M1 pressure conditions was considered instead of the M2 because the dated eclogite by García-Ramírez et al. (2017) do not show thermal imprint. Using these values, the PMC rocks suffer and exhumation rate exceeding 6 mm/yr, which are higher than those reported from serpentinite-dominated subduction channels commonly showing decompression rates below 4 mm/yr (Agard et al., 2009; Guillot et al., 2009; Blanco-Quintero et al., 2011b). This approximation precludes the slow rate mechanism during exhumation as a feasible explanation of the observed metamorphic trajectory.

On the other hand, flat-slab geodynamics is also precluded by the abundant record of thick volcanic sequences and magmatism during the Early Cretaceous. At the same time, the trench-ward migration of the continental magmatic arc and the formation of multiple back-arc

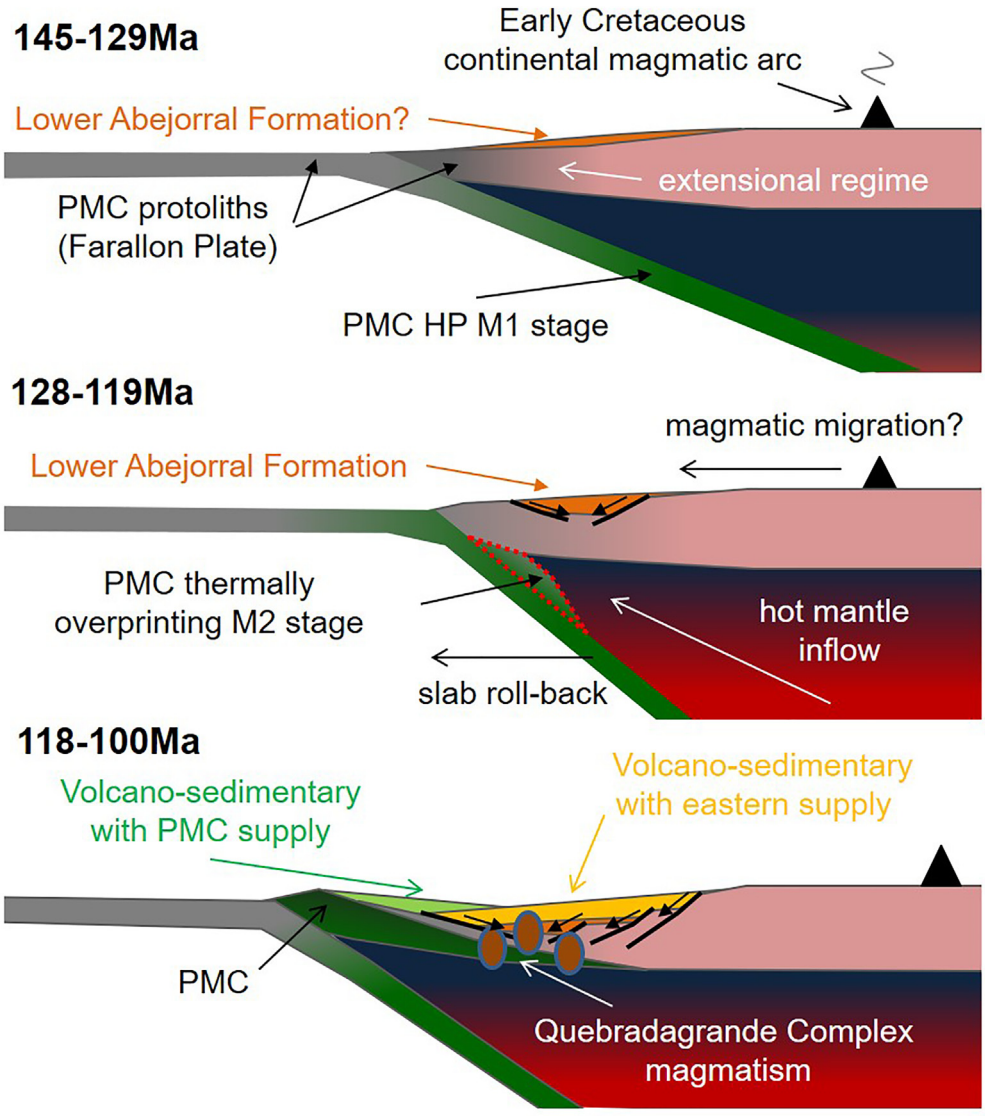

Fig. 13. Schematic cross-section of the tectonic evolution of the Pijao Metamorphic Complex (modified from Avellaneda-Jiménez et al., 2019). M1 stage (HP metamorphism) was associated with a cold subduction regime. Upper amphibolite to HP granulite facies overprinting (M2) is linked to roll-back tectonics triggering hot mantle inflow, trench-ward magmatic arc migration, and multiple back-arc basin development. Subsequent subduction of oceanic crust in an already established warm subduction system allowed prograde amphibolite-facies metamorphism recorded in the western belt of the PMC. See text for discussion.

basins along the Northern Andes, which have been associated with a margin-scale slab roll-back event (Spikings et al., 2015; Avellaneda-Jiménez et al., 2019; Cardona et al., 2019; León et al., 2019a,b; Zapata et al., 2019), also precludes a flat-slab scenario. The latter is also unexpected during oceanic ridge subduction given the ability of young and hot oceanic crust, when subducted, to promote flat slab tectonics triggering upper plate compression and land-ward magmatic arc migration instead (Delong and Fox, 1977; Ramos and Folguera, 2009). Therefore, this mechanism is also considered unfeasible. Within the subduction zone, roll-back tectonics is not only responsible for the thermal modification of the associated subduction system as proposed in world-wide examples (e.g. Phillips et al., 2015; Laurent et al., 2018), but also for rapid exhumation rates in accordance with the PMC evolution (Figs. 12 and 13; e.g. Jolivet et al., 1994; Brun and Faccenna, 2008; Guillot et al., 2009). Short-lived conductive thermal overprint of HP rocks due to hot mantle upwelling triggered by slab roll-back geodynamics have been also constrained by numerical modeling (Sizova et al., 2019), showing that upper amphibolite to HP granulite facies conditions after the HP stage can be achieved before 10 Ma as observed within the PMC.

We consider that the modification of the subduction thermal structure registered in the eastern belt of the PMC, passing from cold (< 10 °C/km) to warmer conditions (10–30 °C/km), might have also influenced the observed prograde amphibolite facies metamorphism registered in the western belt (Fig. 2A and B). We propose that continued warming of the subduction zone due to hot mantle influx, resulted in a thermal structure that allowed the newly entering pieces of the subducting slab to suffer similar metamorphic P-T paths like the ones recorded by rocks associated with warm oceanic crust subduction in the Caribbean region (Fig. 12; e.g. Garcia-Casco et al., 2008a; Blanco-Quintero et al., 2010). We also consider that several units within the regional ECAC may have only recorded the warmer final stages of the subduction system, leading to rocks with a metamorphic history recording only prograde amphibolite facies conditions as those described farther to the north (e.g. Ruíz-Jiménez et al., 2012).

When the metamorphic history described in this contribution is integrated in the context of the widespread Early Cretaceous extensional related magmatic and sedimentary record of the Northern Andes (Cochrane et al., 2014; Spikings et al., 2015; Zapata et al., 2019), the view of a South American margin scale roll-back event during the

Early Cretaceous (reviews in Spikings et al., 2015; Braz et al., 2018; Zapata et al., 2019) gains strong geological support.

6. Conclusions

New fieldwork and petrological constraints from interbedded garnet mica schists, coarse-grained garnet amphibolites, and thermally overprinted eclogites exposed in the western flank of the Central Cordillera of the Colombian Andes, allowed the recognition of three major metamorphic stages M1, M2, and M3.

The M1 high-pressure assemblage consists of garnet + omphacite + phengite + lawsonite, which was overprinted by the M2 upper amphibolite to HP granulite transitional facies stage characterized by the formation of augite + Ti-rich brown amphibole + oligoclase + high Mg# garnet, and small leucocratic segregates associated with partial melting. These rocks are finally retrograded to M3 greenschist to epidote-amphibolite facies conditions during the final exhumation event.

Thermobarometric estimates using isochemical P-T phase diagrams suggest a clockwise P-T path with M1 stage yielding 18.2–24.5 kbar and 465–580 °C, a thermally overprinting M2 stage within 6.5–14.3 kbar and 580–720 °C, and a final retrograde M3 stage below 6.5–11 kbar and 286–400 °C.

Garnet chemistry describes a well-defined X_{grs}/X_{prp} decrease and Mg# enrichment from core to rim, as well as rapid exhumation rates over 6 mm/yr, which argue for a metamorphic gradient modification during prograde metamorphism in a subduction-related setting. The rapid exhumation rates, thermal overprint, and regional geological constraints suggest hot mantle inflow triggered by roll-back tectonics as a feasible mechanism, providing the first report of Cretaceous roll-back-related metamorphism in the Caribbean and Andean realms.

Declaration of Competing Interest

The authors declare that they have no known competing financial interests or personal relationships that could have appeared to influence the work reported in this paper.

Acknowledgments

The authors thank A. García-Casco and an anonymous reviewer for their constructive reviews which substantially improved this article, as well as editor R. Palin for editorial handling. We thank EGEO research group members for fieldwork support and multiple discussions between 2015 and 2019. The National University of Colombia is acknowledged for its financial support, providing execution of the Hermes 30362 project and a travel grant to D. S. Avellaneda-Jiménez for analytical data acquisition at the University of Arizona (Tucson, Arizona). K. Domanik from the University of Arizona is deeply acknowledged for his help during mineral chemistry data acquisition.

Appendix A. Supplementary data

Supplementary data to this article can be found online at https://doi.org/10.1016/j.gsf.2020.09.019.

References

Agard, P., Yamato, P., Jolivet, L., Burov, E., 2009. Exhumation of oceanic blueschists and eclogites in subduction zones: timing and mechanisms. Earth Sci. Rev. 92 (1–2), 53–79.

Avellaneda-Jiménez, D.S., Cardona, A., Valencia, V., Barbosa, J.S., Jaramillo, J.S., Monsalve, G., Ramírez-Hoyos, L., 2019. Erosion and regional exhumation of an early cretaceous subduction/accretion complex in the Colombian Andes. Int. Geol. Rev. https://doi.org/10.1080/00206814.2019.1596042.

Bayona, G., Jiménez, G., Silva, C., Cardona, A., Montes, C., Roncancio, J., Cordani, U., 2010. Paleomagnetic data and K–Ar ages from Mesozoic units of the Santa Marta Massif: A preliminary interpretation for block rotations and translations. J. S. Am. Earth Sci. 29 (4), 817–831.

Blanco-Quintero, I.F., García-Casco, A., Rojas-Agramonte, Y., Rodríguez-Vega, A., Lázaro, C., Iturralde-Vinent, M.A., 2010. Metamorphic evolution of subducted hot oceanic crust (La Corea Melange, Cuba). Am. J. Sci. 310 (9), 889–915.

Blanco-Quintero, I.F., García-Casco, A., Gerya, T.V., 2011a. Tectonic blocks in serpentinite mélange (eastern Cuba) reveal large-scale convective flow of the subduction channel. Geology 39 (1), 79–82.

Blanco-Quintero, I.F., Rojas-Agramonte, Y., García-Casco, A., Kröner, A., Mertz, D.F., Lázaro, C., Blanco-Moreno, J., Renne, P.R., 2011b. Timing of subduction and exhumation in a subduction channel: evidence from slab melts from La Corea mélange (eastern Cuba). Lithos 127, 86–100.

Braz, C., Seton, M., Flament, N., Müller, R.D., 2018. Geodynamic reconstruction of an accreted cretaceous back-arc basin in the Northern Andes. J. Geodyn. 121, 115–132. https://doi.org/10.1016/j.jog.2018.09.008.

Brun, J.P., Faccenna, C., 2008. Exhumation of high-pressure rocks driven by slab rollback. Earth Planet. Sci. Lett. 272 (1–2), 1–7.

Bustamante, A., Juliani, C., Hall, C.M., Essene, E.J., 2011. $^{40}Ar/^{39}Ar$ ages from blueschists of the Jambaló region, Central Cordillera of Colombia: Implications on the styles of accretion in the northern Andes. Geol. Acta 9 (3–4), 351–362.

Bustamante, A., Juliani, A., Essene, E.J., Hall, C.M., Hyppolito, T., 2012. Geochemical constraints on blueschist- and amphibolite-facies rocks of the Central Cordillera of Colombia: the Andean Barragán region. Int. Geol. Rev. 54 (9), 1013–1030. https://doi.org/10.1080/00206814.2011.594226.

Bustamante, C., Bustamante, A., 2019. Two Cretaceous subduction events in the Central Cordillera: Insights from the high P–low T metamorphism. In: Gómez, J., Pinilla-Pachon, A.O. (Eds.), The Geology of Colombia. Volume 2 Mesozoic. Servicio Geológico Colombiano, Publicaciones Geológicas Especiales 36 https://doi.org/10.32685/pub.esp.36.2019.14 (14 p. Bogotá).

Bustamante, C., Archanjo, C.J., Cardona, A., Vervoort, J.D., 2016. Late Jurassic to early cretaceous plutonism in the Colombian Andes: A record of long-term arc maturity. Geol. Soc. Am. Bull. 128 (11−12), 1762–1779.

Cardona, A., León, S., Jaramillo, J.S., Valencia, V., Zapata, S., Pardo-Trujillo, A., Schmitt, A.K., Mejía, D., Arenas, J.C., 2019. Cretaceous record from a Mariana to an Andean-type margin in the Central Cordillera of the Colombian Andes. In: Gómez, J., Pinilla-Pachón, A.O. (Eds.), The Geology of Colombia. Servicio Geológico Colombiano. Publicaciones Geológicas Especiales, 36, Bogotá, pp. 353–395 https://doi.org/10.32685/pub.esp.36.2019.10.

Cathelineau, M., 1988. Cation site occupancy in chlorites and illites as a function of temperature. Clay Miner. 23 (4), 471–485.

Cochrane, R., Spikings, R., Gerdes, A., Winkler, W., Ulianov, A., Mora, A., Chiaradia, M., 2014. Distinguishing between in-situ and accretionary growth of continents along active margins. Lithos 202, 382–394.

Connolly, J.A., 2005. Computation of phase equilibria by linear programming: a tool for geodynamic modeling and its application to subduction zone decarbonation. Earth Planet. Sci. Lett. 236 (1), 524–541.

Dale, J., Powell, R., White, R.W., Elmer, F.L., Holland, T.J.B., 2005. A thermodynamic model for Ca–Na clinoamphiboles in Na_2O–CaO–FeO–MgO–Al_2O_3–SiO_2–H_2O–O for petrological calculations. J. Metamorph. Geol. 23 (8), 771–791.

Delong, S.E., Fox, P.J., 1977. Geological consequences of ridge subduction. In: Talwani, M., Pitman, W.C. (Eds.), Island Arcs, Deep Sea Trenches and Back-Arc Basins. vol. 1. American Geophysical Union, Washington, DC, pp. 221–228.

Ernst, W.G., 1988. Tectonic history of subduction zones inferred from retrograde blueschist PT paths. Geology 16 (12), 1081–1084.

Ernst, W.G., 2010. Subduction-zone metamorphism, calc-alkaline magmatism, and convergent-margin crustal evolution. Gondwana Res. 18 (1), 8–16. https://doi.org/10.1016/j.gr.2009.05.010.

Ernst, W.G., Liu, J., 1998. Experimental phase-equilibrium study of Al-and Ti-contents of calcic amphibole in MORB—A semiquantitative thermobarometer. Am. Mineral. 83 (9–10), 952–969.

Escuder-Viruete, J., Castillo-Carrión, M., 2016. Subduction of fore-arc crust beneath an intra-oceanic arc: the high-P Cuaba mafic gneisess and amphibolites of the Rio San Juan complex, Dominican Republic. Lithos 262, 298–319.

Escuder-Viruete, J., Joubert, M., Urien, P., Friedman, R., Weis, D., Ullrich, T., Pérez-Estaún, A., 2008. Caribbean island-arc rifting and back-arc basin development in the late cretaceous: geochemical, isotopic and geochronological evidence from Central Hispaniola. Lithos 104 (1–4), 378–404.

Escuder-Viruete, J., Valverde-Vaquero, P., Rojas-Agramonte, Y., Jabites, J., Pérez-Estaún, A., 2013. From intra-oceanic subduction to arc accretion and arc-continent collision: Insights from the structural evolution of the Río San Juan metamorphic complex, northern Hispaniola. J. Struct. Geol. 46, 34–56.

Evans, T.P., 2004. A method for calculating effective bulk composition modification due to crystal fractionation in garnet-bearing schist: implications for isopleth thermobarometry. J. Metamorph. Geol. 22 (6), 547–557.

Faryad, S.W., Baldwin, S.L., Jedlicka, R., Ježek, J., 2019. Two-stage garnet growth in coesite eclogite from the southeastern Papua New Guinea (U) HP terrane and its geodynamic significance. Contrib. Mineral. Petrol. 174 (9), 73.

Gaidies, F., Abart, R., De Capitani, C., Schuster, R., Connolly, J.A.D., Reusser, E., 2006. Characterization of polymetamorphism in the Austroalpine basement east of the Tauern Window using garnet isopleth thermobarometry. J. Metamorph. Geol. 24 (6), 451–475.

García-Casco, A., Lázaro, C., Rojas-Agramonte, Y., Kröner, A., Torres-Roldán, R.L., Núñez, K., Neubauer, F., Millán, G., Blanco-Quintero, I., 2008a. Partial melting and counterclockwise P–T path of subducted oceanic crust (Sierra del Convento mélange, Cuba). J. Petrol. 49 (1), 129–161.

García-Casco, A., Iturralde-Vinent, M.A., Pindell, J., 2008b. Latest cretaceous collision/accretion between the Caribbean Plate and Caribeana: origin of metamorphic terranes in the Greater Antilles. Int. Geol. Rev. 50 (9), 781–809.
García-Ramírez, C.A., Ríos-Reyes, C.A., Castellanos-Alarcón, O.M., Mantilla-Figueroa, L.C., 2017. Petrology, geochemistry and geochronology of the Arquía Complex's metabasites at the Pijao-Génova sector, Central Cordillera, Colombian Andes. Boletín Geol. 39 (1), 105–126.
Gómez, J., Montes, N.E., Nivia, A., Diederix, H., compilers, 2014. Geological Map of Colombia. Scale 1:1,000,000. Bogotá, Colombian Geological Survey.
González, I.H., 1997. Metagabros y Eclogitas Asociadas en el Area de Barragan, Departamento del Valle, Colombia. Geol. Colomb. 22, 151–170.
Green, E., Holland, T., Powell, R., 2007. An order-disorder model for omphacitic pyroxenes in the system jadeite-diopside-hedenbergite-acmite, with applications to eclogitic rocks. Am. Mineral. 92 (7), 1181–1189.
Green, E.C.R., White, R.W., Diener, J.F.A., Powell, R., Holland, T.J.B., Palin, R.M., 2016. Activity–composition relations for the calculation of partial melting equilibria in metabasic rocks. J. Metamorph. Geol. 34 (9), 845–869.
Guillot, S., Hattori, K., Agard, P., Schwartz, S., Vidal, O., 2009. Exhumation processes in oceanic and continental subduction contexts: a review. Subduction Zone Geodynamics. Springer, Berlin, Heidelberg, pp. 175–205.
Gutiérrez, J.B.R., 2019. Aportes al conocimiento del Magmatismo de la Cordillera Central de Colombia en su Flanco Oriental: Área geotérmica de San Diego, Samaná, Caldas. Boletín Geol. 41 (2), 45–70 (in Spanish).
Hawthorne, F.C., Oberti, R., Harlow, G.E., Maresch, W.V., Martin, R.F., Schumacher, J.C., Welch, M.D., 2012. Nomenclature of the amphibole supergroup. Am. Mineral. 97 (11–12), 2031–2048.
Hey, M.H., 1954. A new review of the chlorites. Mineral. Mag. J. Mineral. Soc. 30 (224), 277–292.
Hincapié-Gómez, S., Cardona, A., Jiménez, G., Monsalve, G., Ramírez-Hoyos, L., Bayona, G., 2017. Paleomagnetic and gravimetrical reconnaissance of cretaceous volcanic rocks from the western Colombian Andes: paleogeographic connections with the Caribbean Plate. Stud. Geophys. Geod. 62, 1–27.
Holland, T., Powell, R., 2003. Activity–composition relations for phases in petrological calculations: an asymmetric multicomponent formulation. Contrib. Mineral. Petrol. 145 (4), 492–501.
Holland, T.J.B., Powell, R., 1998. An internally consistent thermodynamic data set for phases of petrological interest. J. Metamorph. Geol. 16 (3), 309–343.
Jaramillo, J.S., Cardona, A., León, S., Valencia, V., Vinasco, C., 2017. Geochemistry and geochronology from cretaceous magmatic and sedimentary rocks at 6° 35′ N, western flank of the Central cordillera (Colombian Andes): Magmatic record of arc growth and collision. J. S. Am. Earth Sci. 76, 460–481.
John, T., Scherer, E.E., Schenk, V., Herms, P., Halama, R., Garbe-Schönberg, D., 2009. Subducted seamounts in an eclogite-facies ophiolite sequence: the Andean Raspas complex, SW Ecuador. Contrib. Mineral. Petrol. 159 (2), 265–284.
Jolivet, L., Daniel, J.M., Truffert, C., Goffé, B., 1994. Exhumation of deep crustal metamorphic rocks and crustal extension in arc and back-arc regions. Lithos 33 (1–3), 3–30. https://doi.org/10.1016/0024-4937(94)90051-5.
Jowett, E.C., 1991. Fitting iron and magnesium into the hydrothermal chlorite geothermometer. GAC/MAC/SEG Joint Annual Meeting, Toronto, May 27–29, 1991 (Program with Abstracts 16).
Kerr, A.C., Marriner, G.F., Tarney, J., Nivia, Á., Saunders, A.D., Thirlwall, M.F., Sinton, C.W., 1997. Cretaceous basaltic terranes in western Colombia: Elemental, chronological and Sr–Nd isotopic constraints on petrogenesis. J. Petrol. 38 (6), 677–702.
Krebs, M., Maresch, W.V., Schertl, H.P., Münker, C., Baumann, A., Draper, G., Idleman, B., Trapp, E., 2008. The dynamics of intra-oceanic subduction zones: a direct comparison between fossil petrological evidence (Rio San Juan complex, Dominican Republic) and numerical simulation. Lithos 103 (1–2), 106–137.
Krebs, M., Schertl, H.P., Maresch, W.V., Draper, G., 2011. Mass flow in serpentinite-hosted subduction channels: P–T–t path patterns of metamorphic blocks in the Rio San Juan mélange (Dominican Republic). J. Asian Earth Sci. 42 (4), 569–595.
Laurent, V., Lanari, P., Nair, I., Augier, R., Lahfid, A., Jolivet, L., 2018. Exhumation of eclogite and blueschist (Cyclades, Greece): Pressure-temperature evolution de-termined by thermobarometry and garnet equilibrium modeling. J. Metamorph. Geol. 36, 769–798. https://doi.org/10.1111/jmg.12309.
Lázaro, C., Blanco-Quintero, I.F., Rojas-Agramonte, Y., Proenza, J.A., Núñez-Cambra, K., García-Casco, A., 2013. First description of a metamorphic sole related to ophiolite obduction in the northern Caribbean: geochemistry and petrology of the Güira de Jauco Amphibolite complex (eastern Cuba) and tectonic implications. Lithos 179, 193–210.
Lázaro, C., Blanco-Quintero, I.F., Proenza, J.A., Rojas-Agramonte, Y., Neubauer, F., Núñez-Cambra, K., Garcia-Casco, A., 2016. Petrogenesis and 40Ar/39Ar dating of proto-forearc crust in the early cretaceous Caribbean arc: the La Tinta mélange (eastern Cuba) and its easterly correlation in Hispaniola. Int. Geol. Rev. 58 (8), 1020–1040.
León, S., Cardona, A., Mejía, D., Botello, G.E., Villa, V., Collo, G., Valencia, V., Zapata, S., Avellaneda-Jiménez, D.S., 2019a. Source area evolution and thermal record of an early cretaceous back-arc basin along the northwesternmost Colombian Andes. J. S. Am. Earth Sci. 94, 102229. https://doi.org/10.1016/j.jsames.2019.102229.
León, S., Cardona, A., Jaramillo, J.S., Zapata, S., Avellaneda-Jiménez, D.S., 2019b. Comment on "Origin of pre-Mesozoic xenocrystic zircons in Cretaceous sub-volcanic rocks of the Northern Andes (Colombia): paleogeographic implications for the region" by Cetina et al., 2019. J. S. Am. Earth Sci., 102400 https://doi.org/10.1016/j.jsames.2019.102400.
Liou, J.G., Tsujimori, T., Zhang, R.Y., Katayama, I., Maruyama, S., 2004. Global UHP metamorphism and continental subduction/collision: the Himalayan model. Int. Geol. Rev. 46 (1), 1–27.
Locock, A.J., 2014. An Excel spreadsheet to classify chemical analyses of amphiboles following the IMA 2012 recommendations. Comput. Geosci. 62, 1–11.
Maresch, W.V., Kluge, R., Baumann, A., Pindell, J.L., Krückhans-Lueder, G., Stanek, K., 2009. The occurrence and timing of high-pressure metamorphism on Margarita Island, Venezuela: a constraint on Caribbean-South America interaction. Geol. Soc. Lond., Spec. Publ. 328 (1), 705–741.
Maya, M., González, H., 1995. Unidades litodémicas en la Cordillera Central de Colombia. Bol. Geol. Ingeom. 35, 43–57 (in Spanish).
McCourt, W., Aspden, J., Brook, M., 1984. New geological and geochronological data from the Colombian Andes: continental growth by multiple accretion. J. Geol. Soc. Lond. 141, 831–845.
McCourt, W.J., Mosquera, D., Nivia, A., Núñez, A., 1985. Geología de la Plancha 243 Armenia. Escala 1:100.000. Versión digital 2009. Ingeominas (in Spanish).
Montes, C., Rodriguez-Corcho, A.F., Bayona, G., Hoyos, N., Zapata, S., Cardona, A., 2019. Continental margin response to multiple arc-continent collisions: the northern Andes-Caribbean margin. Earth Sci. Rev. 102903.
Morimoto, N., 1988. Nomenclature of pyroxenes. Mineral. Petrol. 39 (1), 55–76.
Nivia, A., Marriner, G.F., Kerr, A.C., Tarney, J., 2006. The Quebradagrande complex: A lower cretaceous ensialic marginal basin in the Central Cordillera of the Colombian Andes. J. S. Am. Earth Sci. 21, 423–436.
O'Brien, P.J., Rötzler, J., 2003. High-pressure granulites: formation, recovery of peak conditions and implications for tectonics. J. Metamorph. Geol. 21 (1), 3–20.
Orrego, A., Cepeda, H., Rodríguez, G., 1980. Esquistos glaucofánicos en el área de Jambaló, Cauca (Colombia). Geol. Norandina 1, 5–10 (in Spanish).
Otten, M.T., 1984. The origin of brown hornblende in the Artfjället gabbro and dolerites. Contrib. Mineral. Petrol. 86 (2), 189–199.
Pardo-Trujillo, A., Cardona, A., Giraldo, A.S., León, S., Vallejo, D.F., Trejos-Tamayo, R., Plata, A., Ceballos, J.A., Echeverri, J.S., Barbosa-Espitia, A.A., Slattery, J., Salazar, A.F., Botello, G.E., Celis, S., Osorio-Granada, E., Giraldo-Villegas, C.A., 2020. Sedimentary record of the Cretaceous-Paleogene arc-continent collision in the northwestern Colombian Andes: Insights from stratigraphic and provenance constraints. Sediment. Geol. 401, 105627.
Phillips, G., Offler, R., Rubatto, D., Phillips, D., 2015. High-pressure metamorphism in the southern New England Orogen: implications for long-lived accretionary orogenesis in eastern Australia. Tectonics, 34 https://doi.org/10.1002/2015TC003920.
Pindell, J., Kennan, L., Maresch, W.V., Stanek, K., Draper, G., Higgs, R., 2005. Plate-kinematics and crustal dynamics of circum-Caribbean arc-continent interactions: tectonic controls on basin development in Proto-Caribbean margins. Special Papers-Geological Society of America. vol. 394, p. 7.
Pindell, J.L., Kennan, L., 2009. Tectonic evolution of the Gulf of Mexico, Caribbean and northern South America in the mantle reference frame: an update. Geol. Soc. Lond., Spec. Publ. 328 (1), 1–55.
Raase, P., 1974. Al and Ti contents of hornblende, indicators of pressure and temperature of regional metamorphism. Contrib. Mineral. Petrol. 45 (3), 231–236.
Ramos, V.A., Folguera, A., 2009. Andean flat-slab subduction through time. Geol. Soc. Lond., Spec. Publ. 327 (1), 31–54.
Restrepo, J.J., Toussaint, J.F., 1976. Edades radiométricas de algunas rocas de Antioquia, Colombia. Publicacion Especial Geología. vol. 12. Universidad Nacional de Medellin, pp. 1–11 (in Spanish).
Rieder, M., Cavazzini, G., D'yakonov, Y.S., Frank-Kamenetskii, V.A., Gottardi, G., Guggenheim, S., Koval, P.V., Müller, G., Neiva, A.M.R., Rodoslovich, E.W., Robert, J.L., Sassi, F.P., Takeda, H., Weiss, Z., Wones, D.R., 1998. Nomenclature of the micas. Clay Clay Miner. 46 (5), 586–595.
Rodríguez, G., Arango, M.I., 2013. Reinterpretación geoquímica y radiométrica de las metabasitas del Complejo Arquía. Boletín Geol. 35 (2), 65–81 (in Spanish).
Ruíz-Jiménez, E., Blanco-Quintero, I.F., Toro, L.M., Moreno, M., Garcia, A., Morata, D., Goméz, A., 2012. Geoquímica y Petrología de las metabasitas del Complejo Arquía (Municipio de Santafé de Antioquia y Río Arquía, Colombia): Implicaciones geodinámicas. Boletín Ciencias de la Tierra 32, 65–80 (in Spanish).
Sarmiento-Rojas, L.F., Van Wess, L.D., Cloetingh, S., 2006. Mesozoic transtensional basin history of the Eastern Cordillera, Colombian Andes: inferences from tectonic models. J. S. Am. Earth Sci. 21, 383–411. https://doi.org/10.1016/j.jsames.2006.07.003.
Siivola, J., Schmid, R., 2007. A systematic nomenclature for metamorphic rocks: 12. List of mineral abbreviations. Recommendations by the IUGS Subcommission on the Systematics of Metamorphic Rocks. vol. 1 Recommendations, web version of.
Sizova, E., Hauzenberger, C., Fritz, H., Faryad, S.W., Gerya, T., 2019. Late orogenic heating of (ultra) high pressure rocks: Slab Rollback vs. Slab Breakoff. Geosciences 9 (12), 499.
Song, S.G., Yang, J.S., Xu, Z.Q., Liou, J.G., Shi, R.D., 2003. Metamorphic evolution of the coesite-bearing ultrahigh-pressure terrane in the North Qaidam, Northern Tibet, NW China. J. Metamorph. Geol. 21 (6), 631–644.
Spear, F.S., 1993. Metamorphic Phase Equilibria and Pressure-Temperature-Time Paths. vol. 1. Mineralogical Society of America, Washington, DC, p. 799.
Spikings, R., Cochrane, R., Villagómez, D., Van der Lelij, R., Vallejo, C., Winkler, W., Beate, B., 2015. The geological history of northwesten South America: from Pangaea to early collision of the Caribbean large Igneous Province (290-75Ma). Gondwana Res. 27, 96–139.
Toussaint, J., 1996. Evolución Geológica de Colombia. Universidad Nacional de Colombia, Medellín 166p (in Spanish).
Toussaint, J.F., Restrepo, J.J., 1978. Edad Cretácea de una anfibolita granatífera de Pijao, Quindío. Publ. Esp. Geol. Univ. Nacional Medellín N°16, p.1 (in Spanish).
Tsujimori, T., Ernst, W.G., 2014. Lawsonite blueschists and lawsonite eclogites as proxies for palaeo-subduction zone processes: a review. J. Metamorph. Geol. 32 (5), 437–454.
Villagómez, D., Spikings, R., 2013. Thermochronology and tectonics of the Central and Western Cordilleras of Colombia: early Cretaceous–Tertiary evolution of the Northern Andes. Lithos 168, 228–249.

Villagómez, D., Spikings, R., Magna, T., Kammer, A., Winkler, W., Unitrán, A., 2011. Geochronology, geochemistry and tectonic evolution of the Western and Central cordilleras of Colombia. Lithos 125 (3–4), 875–896.

Wakabayashi, J., 2004. Tectonic mechanisms associated with P-T paths of regional metamorphism: Alternatives to single-cycle thrusting and heating. Tectonophysics 392, 193–218. https://doi.org/10.1016/j.tecto.2004.04.012.

White, R.W., Powell, R., Holland, T.J.B., 2001. Calculation of partial melting equilibria in the system Na_2O–CaO–K_2O–FeO–MgO–Al_2O_3–SiO_2–H_2O (NCKFMASH). J. Metamorph. Geol. 19 (2), 139–153.

White, R.W., Powell, R., Johnson, T.E., 2014. The effect of Mn on mineral stability in metapelites revisited: new a–x relations for manganese-bearing minerals. J. Metamorph. Geol. 32 (8), 809–828.

Zapata, J.P., Cardona, A., Restrepo, J.J., Martens, U., 2017. Geoquímica y geocronología de las rocas volcánicas básicas y el Gabro de Altamira, Cordillera Occidental (Colombia): Registro de ambientes de Plateau y arco oceánico superpuestos durante el Cretácico. Boletín Geol. 39, 13–30 (in Spanish).

Zapata, S., Cardona, A., Jaramillo, J.S., Patiño, A.M., Valencia, V., León, S., Mejía, D., Pardo-Trujillo, A., Castañeda, J.P., 2019. Cretaceous extensional and compressional tectonics in the Northwestern Andes, prior to the collision with the Caribbean oceanic plateau. Gondwana Res. https://doi.org/10.1016/j.gr.2018.10.008. (in press).

Zhang, X.Z., Wang, Q., Dong, Y.S., Zhang, C., Li, Q.Y., Xia, X.P., Xu, W., 2017. High-pressure granulite facies overprinting during the exhumation of eclogites in the Bangong-Nujiang Suture Zone, Central Tibet: link to Flat-Slab Subduction. Tectonics 36 (12), 2918–2935.

Zhao, G., Cawood, P.A., Wilde, S.A., Lu, L., 2001. High-pressure granulites (retrograded eclogites) from the Hengshan complex, North China Craton: petrology and tectonic implications. J. Petrol. 42 (6), 1141–1170.